JOURNAL OF GUIDANCE, CONTROL, AND DYNAMICS
Vol. 32, No. 2, March–April 2009

Nonlinear Robust Adaptive Control of Flexible Air-Breathing Hypersonic Vehicles

Lisa Fiorentini* and Andrea Serrani†
The Ohio State University, Columbus, Ohio 43210
and
Michael A. Bolender‡ and David B. Doman§
U.S. Air Force Research Laboratory, Wright–Patterson Air Force Base, Ohio 45433

DOI: 10.2514/1.39210

This paper describes the design of a nonlinear robust adaptive controller for a flexible air-breathing hypersonic vehicle model. Because of the complexity of a first-principle model of the vehicle dynamics, a control-oriented model is adopted for design and stability analysis. This simplified model retains the dominant features of the higher-fidelity model, including the nonminimum phase behavior of the flight-path angle dynamics, the flexibility effects, and the strong coupling between the engine and flight dynamics. A combination of nonlinear sequential loop closure and adaptive dynamic inversion is adopted for the design of a dynamic state-feedback controller that provides stable tracking of the velocity and altitude reference trajectories and imposes a desired set point for the angle of attack. A complete characterization of the internal dynamics of the model is derived for a Lyapunov-based stability analysis of the closed-loop system, which includes the structural dynamics. The proposed methodology addresses the issue of stability robustness with respect to both parametric model uncertainty, which naturally arises when adopting reduced-complexity models for control design, and dynamic perturbations due to the flexible dynamics. Simulation results from the full nonlinear model show the effectiveness of the controller.

Nomenclature

$\boldsymbol{B}_i$	=	control effectiveness vectors
C_i^j	=	aerodynamic coefficients
$\bar{c}$	=	mean aerodynamic chord, ft
D	=	drag, lbf/ft
g	=	acceleration due to gravity, ft/s^2
h	=	altitude, ft
h_{ref}	=	altitude reference trajectory, ft
I_{yy}	=	moment of inertia, slug $\cdot$ ft^2/(rad $\cdot$ ft)
k_i	=	controller gains, $i = 1, \ldots, 5$
L	=	lift, lbf/ft
M	=	pitching moment, lbf/ft
m	=	vehicle mass, slug/ft
N_i	=	ith generalized force, ft/s$^2 \cdot \sqrt{\text{slugs}}$/ft
$\mathcal{P}$	=	model parameter set, $\boldsymbol{p} \in \mathcal{P}$
$\boldsymbol{p}$	=	vector of uncertain parameters of the control-design model
$\boldsymbol{p}^0$	=	nominal value of $\boldsymbol{p}$
Q	=	pitch rate, rad/s
Q_{cmd}	=	command trajectory for Q, rad/s
$\bar{q}$	=	dynamic pressure, psf
S	=	reference area, ft^2
T	=	thrust, lbf/ft
$\boldsymbol{u}$	=	control input
V	=	velocity, ft/s
V_{ref}	=	velocity reference trajectory, ft/s
$\boldsymbol{y}$	=	regulated output
W_i	=	control Lyapunov function
$\boldsymbol{x}$	=	rigid-body state
$\boldsymbol{x}^*$	=	rigid-body trim condition
$\boldsymbol{y}_{\text{ref}}$	=	reference output
z_T	=	thrust moment arm, ft
α	=	angle of attack, rad
α_{cmd}	=	command trajectory for α, rad
Γ_i	=	matrices of adaptation gains
γ	=	flight-path angle, rad
γ_{cmd}	=	command trajectory for γ, rad
δ_c	=	canard angular deflection, rad
δ_e	=	elevator angular deflection, rad
ζ_i	=	damping ratio for elastic mode η_i
$\boldsymbol{\eta}$	=	modal coordinate
η_i	=	ith generalized elastic coordinate, ft $\cdot \sqrt{\text{slugs}}$/ft
$\dot{\eta}_i$	=	time derivative of η_i, ft/s $\cdot \sqrt{\text{slugs}}$/ft
$\boldsymbol{\eta}^*$	=	modal coordinate trim condition
Θ_i	=	convex controller parameter sets, $\boldsymbol{\theta}_i \in \Theta_i$, $i = 1, 2, 3$
Θ	=	overall controller parameter set, $\Theta = \Theta_1 \times \Theta_2 \times \Theta_3$
$\boldsymbol{\theta}_i$	=	vector of model parameters, function of $\boldsymbol{p}$
$\hat{\boldsymbol{\theta}}_i$	=	vector of controller parameters
$\Xi_0^{\tilde{x}}$, $\Xi_0^{\tilde{\eta}}$	=	sets of initial conditions for the state variables $\tilde{\boldsymbol{x}}$, $\tilde{\boldsymbol{\eta}}$
ρ	=	air density, slugs/ft^3
σ_i	=	scaling factors of the control Lyapunov functions
Φ	=	fuel equivalence ratio
$\boldsymbol{\Psi}_i$	=	regressors
ω_i	=	natural frequency for elastic mode η_i, rad/s
$\tilde{\bullet}$	=	error variable, for example, $\tilde{h} = h - h_{\text{ref}}$

Received 19 June 2008; revision received 3 November 2008; accepted for publication 6 November 2008.

*Graduate Student, Department of Electrical and Computer Engineering, 2015 Neil Avenue, Student Member AIAA.
†Associate Professor, Department of Electrical and Computer Engineering, 2015 Neil Avenue, Member AIAA.
‡Aerospace Engineer, Air Vehicles Directorate, 2210 Eighth Street, Suite 21. Senior Member AIAA.
§Senior Aerospace Engineer, Air Vehicles Directorate, 2210 Eighth Street, Suite 21. Associate Fellow AIAA.

I. Introduction

AIR-BREATHING hypersonic vehicles are intended to be a reliable and cost-effective technology for access to space. In the past few years, a considerable effort has been made by the U.S. Air Force and NASA to further their development and design. Notwithstanding the recent success of NASA's X-43A experimental vehicle, the design of robust guidance and control systems for hypersonic vehicles is still an open problem due to the peculiarity of the vehicle dynamics. The slender geometries and light structures

required for these aircraft cause significant flexible effects, and strong coupling between propulsive and aerodynamic forces results from the integration of the scramjet engine. In addition, because of the variability of the vehicle characteristics with flight conditions (for example, thermal effects on the structure), significant uncertainties affect the vehicle model [1–3]. A thorough survey of difficulties encountered in the modeling and control of hypersonic vehicles, with a focus on aerothermoelasticity, is given in McNamara and Friedmann [4].

For the design of guidance and control systems for hypersonic vehicles based on linearized dynamical models, several results are available in the literature that consider control solutions of various complexity. The pivotal early works of Schmidt [5,6] employed classic and multivariable linear control for the longitudinal model of the vehicle dynamics developed in Chavez and Schmidt [1,2]. Active structural damping based on Kalman filtering was proposed in Heeg et al. [7]. Subsequent research efforts have considered, for generic vehicle models, the application of $\mathcal{H}_\infty$ design and μ-synthesis methods [8], gain-scheduling and linear parameter-varying control [9,10], and model reference adaptive control [11]. Implicit model-following control methods have been considered in [12–15] for linearized versions of the first-principle model developed by Bolender and Doman [3], and adaptive control techniques have been considered in Kuipers et al. [16] for the computational fluid dynamics based model of Mirmirani et al. [17]. Finally, some aspects of the control system design for NASA's Hyper-X vehicle [18,19] are presented in Davidson et al. [20].

As far as nonlinear control design is concerned, conventional and adaptive sliding-mode control [21,22] and robust inversion-based design [23,24] have been proposed in the literature for simpler vehicle models than the one considered in this paper, which is based on the Bolender and Doman model [3]. In particular, the specific plant models employed in the aforementioned references do not include the structural dynamics, the elevator-to-lift coupling, and the coupling between thrust and pitch moment due to the underslung location of the engine. Indeed, as discussed in [3,25,26], it is the presence of these interactions that render many of the traditional design methodologies unsuitable or difficult to apply to this class of vehicle. For example, elevator-to-lift coupling generates exponentially unstable zero dynamics (with respect to either altitude or flight-path angle as a controlled output) that complicate the design of controllers based on dynamic inversion.

For the Bolender and Doman model, a nonlinear controller that resorts to approximate feedback linearization was proposed in Parker et al. [27]. The approach pursued in that work considered the development of a simplified model for control design in which the flexible dynamics and certain dynamic couplings of interest were strategically ignored in order for the standard assumptions for the applicability of dynamic inversion to hold. With the aid of an external control loop, the nonlinear controller was able to provide stable tracking for a sizable flight envelope, albeit without a formal proof of stability in the presence of flexible dynamics, which were regarded as dynamic perturbations. Furthermore, the fact that the controller was based on the inversion of a reduced-order model naturally prompted the issue of evaluating the robustness of the scheme with respect to parameter and dynamic model uncertainty. However, the complexity of the control law itself rendered such an assessment prohibitive from an analytical standpoint.

Building upon our recent work [28,29], we present here a complete robust adaptive nonlinear control design for the model by Bolender and Doman [3] and Williams et al [30]. A nonlinear controller based on a combination of robust adaptive dynamic inversion and sequential loop closure (i.e., backstepping) [31,32] is designed to achieve robust tracking of altitude and velocity references and regulation of the angle of attack to a desired set point.

Similarly to Parker et al. [27], a simplified model derived from curve-fitted approximations of the aerodynamic and propulsive forces is used for control design. In contrast to [27], however, this control-oriented model retains the dominant features of the higher-fidelity model, which are problematic for control design, including the nonminimum phase behavior of the flight-path angle dynamics, flexibility effects, and coupling between the propulsion system and the airframe. Because measurements of the flexible states are not assumed to be available for feedback, the controller developed in this paper makes use of feedback from the rigid-body states only and is designed assuming a perfectly rigid body, by initially keeping the flexible dynamics "frozen" at a nominal trim condition. The stability analysis of the feedback interconnection of the controller and the overall system is then performed using the full control-design model, which does contain the flexible states.

Because the controller *does not* depend on the model parameters, the design satisfactorily addresses the issue of stability robustness with respect to parameter model uncertainties. In addition, because the proof of stability of the closed-loop system includes the flexible dynamics, robustness with respect to the considered class of dynamic uncertainty is also demonstrated. In contrast to a design based on linearized models, the approach of this paper yields a guaranteed domain of attraction for given ranges of parameter variations. A comparative simulation analysis with the approximate dynamic inversion controller of [27], conducted on the original first-principle model, confirms the validity of the proposed approach.

An important contribution of the paper is the complete characterization of the nonlinear internal dynamics of the Bolender and Doman model with respect to velocity, altitude, and angle of attack as the regulated outputs. The derivation of the internal dynamics, albeit ostensively elaborate, is an indispensable element of the Lyapunov-based stability analysis of the nonlinear closed-loop model, comprehensive of the flexible dynamics, presented in this work. The availability of this analytical tool, in particular, allows the assessment of the gain margins of the closed-loop system and gives guidelines for tuning the controller gains. This is a fundamental aspect of the design process, as it is shown in this paper that the admissible range for the controller gains differ dramatically from the range resulting from an analysis based exclusively on the rigid-body dynamics [21–24,28,29].

In this paper, a canard is assumed to be available as a control effector, in addition to an elevator that acts as the primary aerodynamic control surface. The beneficial role of a canard in counteracting the strong nonminimum phase characteristic of the flight-path angle dynamics was discussed in [27]. It is recognized that there are other approaches that redefine the controlled variables; however, we are interested in demonstrating the benefits of an overactuated system. Work is currently being done to address the issue of nonlinear control design when the elevator is the only available aerodynamic control surface.

II. Vehicle Model

Two distinct models of the longitudinal dynamics of the vehicle are considered: a higher-fidelity simulation model (SM) is used exclusively for closed-loop simulation, whereas a reduced-complexity control-design model (CDM) is employed for control design and a quantitative stability analysis of the closed-loop system. Apart from differences in the actual models, the SM and CDM are similar to the so-called truth model and curve-fitted model (CFM) in Parker et al. [27]. However, in [27] the control design was performed on the basis of a further simplified control-oriented model obtained by removing the flexible states, the altitude dynamics, and a set of weak couplings from the CFM, whereas in this study all these effects have been retained in the model used for control design. In this regard, the new terminology adopted herein better relates to the focus of the paper, which is on control system design instead of modeling.

A. Simulation Model

The SM adopted in this study is the model developed by Bolender and Doman [3] and Williams et al [30] for the longitudinal dynamics of a flexible air-breathing hypersonic vehicle. The equations of motion, derived using Lagrange's equations, include flexibility effects by modeling the vehicle as a single flexible structure with mass-normalized mode shapes. This assumed-modes model considers a traditional free-beam model [33] of the structure in which the flexible modes are orthogonal to the rigid-body modes;

therefore, the interaction between rigid and flexible dynamics occurs only through the aerodynamic forces, as opposed to the original "heave-coupling model" of [3], which was considered in Parker et al. [27]. The scramjet engine model is taken from Chavez and Schmidt [1]. Assuming a flat Earth and normalizing by the span of the vehicle to unit depth, the equations of motion of the longitudinal dynamics are written in the stability axes as

$$\begin{aligned}
\dot{V} &= \frac{T\cos\alpha - D}{m} - g\sin\gamma \\
\dot{h} &= V\sin\gamma \\
\dot{\gamma} &= \frac{L + T\sin\alpha}{mV} - \frac{g}{V}\cos\gamma \\
\dot{\alpha} &= -\frac{L + T\sin\alpha}{mV} + Q + \frac{g}{V}\cos\gamma \\
\dot{Q} &= \frac{M}{I_{yy}} \\
\ddot{\eta}_i &= -2\zeta_i\omega_i\dot{\eta}_i - \omega_i^2\eta_i + N_i, \quad i = 1,2,3
\end{aligned} \tag{1}$$

This model is composed of five rigid-body state variables $\boldsymbol{x} = [V, h, \gamma, \alpha, Q]^T$, six flexible states $\boldsymbol{\eta} = [\eta_1, \dot{\eta}_1, \eta_2, \dot{\eta}_2, \eta_3, \dot{\eta}_3]^T$ corresponding to the first three bending modes of the fuselage, and three control inputs $\boldsymbol{u} = [\Phi, \delta_e, \delta_c]^T$, whereas the output to be controlled is selected as $\boldsymbol{y} = [V, h]^T$. The fuel equivalence ratio affects the thrust directly and the pitching moment indirectly via coupling between the engine and the airframe. The aerodynamic forces/moments and the generalized elastic forces are influenced by the aerodynamic control surfaces. Finally, the structural dynamics are coupled with the rigid-body dynamics as thrust, lift, drag, and pitching moment depend upon the modal coordinates, whereas the generalized forces depend on the angle of attack. The reader is referred to the cited references for details.

B. Control-Design Model

In the SM, the relationships between the control inputs and controlled outputs do not admit a closed-form representation. Following Parker et al. [27], a simplified model has been derived for control design and stability analysis. The resulting nonlinear model, albeit still quite complex, offers the advantage of being analytically tractable, while retaining the relevant dynamical features of the simulation model. The approximations of the forces and moments employed in the CDM are given as follows:

$$\begin{aligned}
&T \approx \bar{q}S[C_{T,\Phi}(\alpha)\Phi + C_T(\alpha) + \boldsymbol{C}_T^{\eta}\boldsymbol{\eta}], \qquad L \approx \bar{q}SC_L(\alpha, \boldsymbol{\delta}, \boldsymbol{\eta}) \\
&D \approx \bar{q}SC_D(\alpha, \boldsymbol{\delta}, \boldsymbol{\eta}), \qquad M \approx z_T T + \bar{q}\,\bar{c}\,SC_M(\alpha, \boldsymbol{\delta}, \boldsymbol{\eta}) \\
&N_i \approx \bar{q}S[N_i^{\alpha^2}\alpha^2 + N_i^{\alpha}\alpha + N_i^{\delta_e}\delta_e + N_i^{\delta_c}\delta_c + N_i^0 + \boldsymbol{N}_i^{\eta}\boldsymbol{\eta}] \\
&\quad i = 1,2,3
\end{aligned} \tag{2}$$

where $\boldsymbol{\delta} = [\delta_c, \delta_e]^T$, and

$$\begin{aligned}
C_{T,\Phi}(\alpha) &= C_T^{\Phi\alpha^3}\alpha^3 + C_T^{\Phi\alpha^2}\alpha^2 + C_T^{\Phi\alpha}\alpha + C_T^{\Phi} \\
C_T(\alpha) &= C_T^3\alpha^3 + C_T^2\alpha^2 + C_T^1\alpha + C_T^0 \\
C_M(\alpha, \boldsymbol{\delta}, \boldsymbol{\eta}) &= C_M^{\alpha^2}\alpha^2 + C_M^{\alpha}\alpha + C_M^{\delta_e}\delta_e + C_M^{\delta_c}\delta_c + C_M^0 + \boldsymbol{C}_M^{\eta}\eta \\
C_L(\alpha, \boldsymbol{\delta}, \boldsymbol{\eta}) &= C_L^{\alpha}\alpha + C_L^{\delta_e}\delta_e + C_L^{\delta_c}\delta_c + C_L^0 + \boldsymbol{C}_L^{\eta}\boldsymbol{\eta} \\
C_D(\alpha, \boldsymbol{\delta}, \boldsymbol{\eta}) &= C_D^{\alpha^2}\alpha^2 + C_D^{\alpha}\alpha + C_D^{\delta_e^2}\delta_e^2 + C_D^{\delta_e}\delta_e + C_D^{\delta_c^2}\delta_c^2 \\
&\quad + C_D^{\delta_c}\delta_c + C_D^0 + \boldsymbol{C}_D^{\eta}\boldsymbol{\eta}. \\
\boldsymbol{C}_j^{\eta} &= [\,C_j^{\eta_1} \quad 0 \quad C_j^{\eta_2} \quad 0 \quad C_j^{\eta_3} \quad 0\,], \quad j = T, M, L, D \\
\boldsymbol{N}_i^{\eta} &= [\,N_i^{\eta_1} \quad 0 \quad N_i^{\eta_2} \quad 0 \quad N_i^{\eta_3} \quad 0\,], \quad i = 1,2,3
\end{aligned} \tag{3}$$

In contrast to [27], the thrust, lift, drag, and moment coefficients of the CDM depend explicitly on the elastic modes. Note also that the CDM includes lift due to the elevator and the effect of the thrust on the pitching moment.

In developing the controller and assessing its closed-loop behavior, it is assumed that all of the coefficients of the CDM are subject to uncertainty, apart from obvious parameters corresponding to physically measurable quantities or known constants. The vector of all uncertain parameters, denoted by $\boldsymbol{p} \in \mathbb{R}^m$, includes the vehicle inertial parameters and the coefficients that appear in the force and moment approximations (that is, $C_T^{(\cdot)}$, $C_M^{(\cdot)}$, and so on). The nominal value of $\boldsymbol{p}$ is denoted by $\boldsymbol{p}^0$. It is assumed that $\boldsymbol{p} \in \mathcal{P}$, where $\mathcal{P}$ is a compact convex set that represents the admissible range of variation of $\boldsymbol{p}$ such that $\boldsymbol{p}^0$ lies in its interior. For simplicity, in this paper a maximum uniform variation within 40% of the nominal value has been considered, yielding the parameter set $\mathcal{P} = \{\boldsymbol{p} \in \mathbb{R}^m | 0.6p_i^0 \le p_i \le 1.4p_i^0, \quad i = 1 \cdots m\}$. The natural frequencies, ω_i, of the flexible dynamics depend on the mass of the vehicle, which decreases as fuel is consumed. Because this variation occurs on a slower time scale than the speed of the references to be tracked, for the purpose of control design the mass has been considered constant during each tracking maneuver. However, both the vehicle mass and the natural frequencies of the flexible dynamics have been considered as uncertain parameters ranging within the intervals given in Table 1 of Sigthorsson et al. [15] corresponding to a 100% variation in fuel level. Note that these values remain within the assumed 40% uncertainty about the nominal value.

III. Nonlinear Controller Design

A. Control Objectives and Problem Formulation

The goal pursued in this study is to design a dynamic controller of the form

$$\dot{\hat{\boldsymbol{\theta}}} = F(\hat{\boldsymbol{\theta}}, \boldsymbol{x}, \boldsymbol{y}_{\text{ref}}), \quad \hat{\boldsymbol{\theta}} \in \mathbb{R}^{\nu} \qquad \boldsymbol{u} = H(\hat{\boldsymbol{\theta}}, \boldsymbol{x}, \boldsymbol{y}_{\text{ref}}) \tag{4}$$

using feedback from the rigid-body states only to steer the output of system (1) from a given set of initial values of velocity and altitude to desired trim conditions V^* and h^* along reference trajectories $\boldsymbol{y}_{\text{ref}}(t) = [V_{\text{ref}}(t), h_{\text{ref}}(t)]^T$, assumed to be bounded and with bounded derivatives of any order. In addition, the control system should provide asymptotic regulation of the angle of attack to a desired trim value, α^*. The control problem considered in this work takes into account only cruise trajectories and does not consider the ascent or the reentry of the vehicle. As a consequence, the velocity and altitude references and the set point for the angle of attack are generated to satisfy the bounds shown in Table 1, which determine the flight envelope, together with the admissible range for the control inputs. Herein, we denote with $\mathcal{A} \subset \mathbb{R}^{10}$ the admissible range for all variables in Table 1. Desired commands $\gamma_{\text{cmd}}(t)$, $\alpha_{\text{cmd}}(t)$, and $Q_{\text{cmd}}(t)$ will be issued by the controller to regulate the corresponding intermediate state variables. The reference and command trajectories are defined such that their asymptotic values yield the desired trim condition of the rigid-body state, $\boldsymbol{x}^* = [V^*, h^*, 0, \alpha^*, 0]^T$, that is, $\lim_{t\to\infty} V_{\text{ref}}(t) = V^*$, $\lim_{t\to\infty} h_{\text{ref}}(t) = h^*$, and $\lim_{t\to\infty} \alpha_{\text{cmd}}(t) = \alpha^*$, whereas $\lim_{t\to\infty} \gamma_{\text{cmd}}(t) = 0$ and $\lim_{t\to\infty} Q_{\text{cmd}}(t) = 0$. Consequently, the tracking error to be regulated to zero is defined as $\tilde{x} = [\tilde{V}, \tilde{h}, \tilde{\gamma}, \tilde{\alpha}, \tilde{Q}]^T := [V - V_{\text{ref}}, h - h_{\text{ref}}, \gamma - \gamma_{\text{cmd}}, \alpha - \alpha_{\text{cmd}}, Q - Q_{\text{cmd}}]^T$.

Table 1 Admissible range, $\mathcal{A}$, for states, inputs, dynamic pressure and Mach number

Variable	Min. value	Max. vValue
V	7500 ft/s	11,000 ft/s
h	70,000 ft	13,5000 ft
γ	−3 deg	3 deg
α	−5 deg	10 deg
Q	−10 deg/s	10 deg/s
Φ	0.05	1.5
δ_c	−20 deg	20 deg
δ_e	−20 deg	20 deg
$\bar{q}$	500 psf	2000 psf
M	7	12

It should be noted that, once the desired trim condition for the rigid-body state is selected, the corresponding trim values $\boldsymbol{u}^* = [\Phi^*, \delta_e^*, \delta_c^*]^T$ and $\boldsymbol{\eta}^* = [\eta_1^*, 0, \eta_2^*, 0, \eta_3^*, 0]^T$ for the control input and the flexible states, respectively, cannot be determined exactly due to parameter uncertainty. The aim of the stability analysis of the closed-loop system is to prove that all state trajectories remain bounded for all possible values of $\boldsymbol{p} \in \mathcal{P}$, whereas $\tilde{\boldsymbol{x}}(t)$ and $\tilde{\boldsymbol{\eta}}(t)$ vanish asymptotically.

For the purpose of control design and stability analysis, it is convenient to formulate the specification on the initial conditions of the rigid-body dynamics in terms of the error variables, $\tilde{\boldsymbol{x}}(0)$, rather than in terms of $\boldsymbol{x}(0)$. In particular, it is assumed that $\tilde{\boldsymbol{x}}(0) \in \Xi_0^{\tilde{x}}$, where $\Xi_0^{\tilde{x}} \subset \mathbb{R}^5$ is a *given* compact set. Similarly, for the initial condition of the flexible dynamics and the state of the controller, it is assumed that $\tilde{\boldsymbol{\eta}}(0) \in \Xi_0^{\tilde{\eta}}$ and $\hat{\boldsymbol{\theta}}(0) \in \Theta$ for given compact sets $\Xi_0^{\tilde{\eta}} \subset \mathbb{R}^6$ and $\Theta \subset \mathbb{R}^{\nu}$. First, the controller will be designed to guarantee that for any $[\tilde{x}(0), \hat{\boldsymbol{\theta}}(0)]^T, \in \Xi_0^{\tilde{x}} \times \Theta$, the trajectory $[\tilde{\boldsymbol{x}}(t), \hat{\boldsymbol{\theta}}(t)]^T$ of the closed-loop CDM remains bounded and $\tilde{\boldsymbol{x}}(t)$ converges to the origin for all $\boldsymbol{p} \in \mathcal{P}$ when the flexible dynamics are frozen at the trim condition $\boldsymbol{\eta} = \boldsymbol{\eta}^*$, that is, $\tilde{\boldsymbol{\eta}} = 0$. Then, the objective of the stability analysis in Sec. IV is to give conditions under which, for the same controller, the boundedness of all closed-loop trajectories and the error regulation continue to hold when $\boldsymbol{\eta} = \tilde{\boldsymbol{\eta}} + \boldsymbol{\eta}^*$ for all initial conditions $[\tilde{\boldsymbol{x}}(0), \tilde{\boldsymbol{\eta}}(0), \hat{\boldsymbol{\theta}}(0)]^T \in \Xi_0^{\tilde{x}} \times \Xi_0^{\tilde{\eta}} \times \Theta$. The performance of the controller is then verified in simulation on the original SM.

B. Controller Design

The starting point is the decomposition of the equations of motion into functional subsystems, namely, the horizontal translation dynamics (the velocity subsystem), the vertical translation dynamics (the altitude and flight-path angle subsystem), and the rotational dynamics (the angle of attack and pitch rate subsystem). Each subsystem is controlled separately using the available inputs at that level and intermediate virtual control commands, as shown in Fig. 1. In particular, a control law with adaptive drag compensation is derived for the velocity subsystem by controlling thrust from the fuel equivalence ratio input, Φ. The altitude dynamics are controlled through the flight-path angle by means of the command γ_{cmd} derived from the altitude reference trajectory. The canard deflection, δ_c, and the angle-of-attack serve, respectively, as a direct and a virtual control input to the flight-path angle dynamics. Because of the fact that the control authority of the canard on the flight-path angle dynamics is significantly smaller than the one of the angle of attack, the main control action will be performed through the command α_{cmd}. The role of the canard is to adaptively decouple lift from elevator commands (thus rendering the system minimum phase), to enforce the equilibrium at the desired trim condition, and to provide a supplementary stabilizing action. Finally, the rotational dynamics are controlled through the pitch moment by means of the elevator

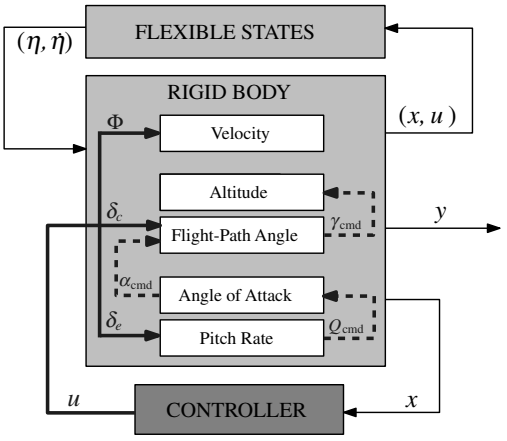

Fig. 1 Block diagram of the control architecture showing direct control inputs Φ, δ_c, and δ_e (bold solid lines) and virtual control inputs γ_{cmd}, α_{cmd}, and Q_{cmd} (dashed lines).

deflection, δ_e. At each step of the design, a control Lyapunov function candidate is selected and a robust adaptive control law is designed on its basis. The stability of the closed-loop rigid-body dynamics is assessed once the construction of the overall controller has been completed.

1. *Adaptive Controller for the Velocity Subsystem*

The controller for the velocity loop is derived by using robust adaptive dynamic inversion. Substituting the expression of T in Eq. (2) into the first equation of Eq. (1), the velocity error dynamics become

$$m\dot{\tilde{V}} = \bar{q}S[C_{T,\Phi}(\alpha)\Phi + C_T(\alpha) + \boldsymbol{C}_T^{\eta}\boldsymbol{\eta}]\cos\alpha - D - mg\sin\gamma - m\dot{V}_{\text{ref}} \tag{5}$$

Defining the vector of uncertain parameters $\boldsymbol{\theta}_1 \in \mathbb{R}^{16}$ as

$$\boldsymbol{\theta}_1 = [C_T^{\Phi\alpha^3}, C_T^{\Phi\alpha^2}, C_T^{\Phi\alpha}, C_T^{\Phi}, C_T^3, C_T^2, C_T^1, (C_T^0 + \boldsymbol{C}_T^{\eta}\boldsymbol{\eta}^*), C_D^{\alpha^2}, C_D^{\alpha}, C_D^{\delta_e^2}, C_D^{\delta_e}, C_D^{\delta_c^2}, C_D^{\delta_c}, (C_D^0 + \boldsymbol{C}_D^{\eta}\boldsymbol{\eta}^*), m]^T$$

Eq. (5) can be written in the linearly parameterized form

$$m\dot{\tilde{V}} = \boldsymbol{\theta}_1^T[\boldsymbol{B}_1(\boldsymbol{x})\Phi - \boldsymbol{\Psi}_1(\boldsymbol{x}, \boldsymbol{u}, \boldsymbol{y}_{\text{ref}})] + \bar{q}S[\boldsymbol{C}_T^{\eta}\cos\alpha - \boldsymbol{C}_D^{\eta}]\tilde{\boldsymbol{\eta}}$$

where the regressor $\boldsymbol{\Psi}_1(\boldsymbol{x}, \boldsymbol{u}, \boldsymbol{y}_{\text{ref}})$ and the input matrix $\boldsymbol{B}_1(\boldsymbol{x})$ are given, respectively, by

$$\boldsymbol{\Psi}_1(\boldsymbol{x}, \boldsymbol{u}, \boldsymbol{y}_{\text{ref}}) = \bar{q}S[\boldsymbol{0}_{1\times4}, -\alpha^3\cos\alpha, -\alpha^2\cos\alpha, -\alpha\cos\alpha, -\cos\alpha, \alpha^2, \alpha, \delta_e^2, \delta_e, \delta_c^2, \delta_c, 1, (g\sin\gamma + \dot{V}_{\text{ref}})/(\bar{q}S)]^T$$

$$\boldsymbol{B}_1(\boldsymbol{x}) = \bar{q}S[\alpha^3\cos\alpha, \alpha^2\cos\alpha, \alpha\cos\alpha, \cos\alpha, \boldsymbol{0}_{1\times12}]^T$$

With considerations analogous to those of [27], it can be shown that controllability of the model implies that $\boldsymbol{\theta}_1^T\boldsymbol{B}_1(\boldsymbol{x}) \neq 0$ for all values of α and $\bar{q}$ within the flight conditions in Table 1 and for all possible values assumed by $\boldsymbol{\theta}_1$ in the convex compact set $\Theta_1 \subset \mathbb{R}^{16}$ obtained by letting the entries of $\boldsymbol{\theta}_1$ vary within the parameter set $\mathcal{P}$. Let $\hat{\boldsymbol{\theta}}_1 \in \mathbb{R}^{16}$ be a vector of estimates of the uncertain parameter, $\boldsymbol{\theta}_1$, and define $\tilde{\boldsymbol{\theta}}_1 := \hat{\boldsymbol{\theta}}_1 - \boldsymbol{\theta}_1$. The control Lyapunov function candidate for the velocity error dynamics is selected as

$$W_1(\tilde{V}, \tilde{\boldsymbol{\theta}}_1) = (\sigma_V/2)(m\tilde{V}^2 + \tilde{\boldsymbol{\theta}}_1^T\Gamma_1^{-1}\tilde{\boldsymbol{\theta}}_1)$$

where $\sigma_V > 0$ is a scaling factor, and $\Gamma_1 \in \mathbb{R}^{16\times16}$ is a diagonal positive definite matrix. Accordingly, the controller for the velocity subsystem is chosen as the dynamical system

$$\begin{aligned}\dot{\hat{\boldsymbol{\theta}}}_1 &= \text{Proj}_{\hat{\boldsymbol{\theta}}_1\in\Theta_1}\{\tilde{V}\Gamma_1[\boldsymbol{B}_1(\boldsymbol{x})\Phi - \boldsymbol{\Psi}_1(\boldsymbol{x}, \boldsymbol{u}, \boldsymbol{y}_{\text{ref}})]\}\\ \Phi &= \frac{1}{\hat{\boldsymbol{\theta}}_1^T\boldsymbol{B}_1(\boldsymbol{x})}[-k_1\tilde{V} + \boldsymbol{\Psi}_1(\boldsymbol{x}, \boldsymbol{u}, \boldsymbol{y}_{\text{ref}})^T\hat{\boldsymbol{\theta}}_1]\end{aligned} \tag{6}$$

with initial conditions $\hat{\boldsymbol{\theta}}_1(0) \in \Theta_1$, where $k_1 > 0$ is a gain parameter and $\text{Proj}_{\hat{\boldsymbol{\theta}}_1\in\Theta_1}(\cdot)$ is a smooth parameter projection [31]. The parameter projection ensures nonsingularity of the control law (6) over the considered envelope of flight conditions.

2. *Adaptive Controller for the $(\tilde{h}, \tilde{\gamma})$ Subsystem*

The outer-loop controller shown in Fig. 2 provides the control law for the altitude and flight-path angle dynamics. To begin, the dynamics of the tracking error $\tilde{h}$ are written as

$$\dot{\tilde{h}} = V\sin\gamma - \dot{h}_{\text{ref}} \approx V_{\text{ref}}\gamma - \dot{h}_{\text{ref}} + \tilde{V}\gamma$$

using the approximation $\sin\gamma \approx \gamma$, which is valid in the range given in Table 1. Choosing the flight-path angle command as $\gamma_{\text{cmd}} = -k_2\tilde{h} + \dot{h}_{\text{ref}}/V_{\text{ref}}$, where $k_2 > 0$ is a gain parameter, yields the dynamics of the altitude tracking error as $\dot{\tilde{h}} = -k_2V_{\text{ref}}\tilde{h} + V_{\text{ref}}\tilde{\gamma} + \tilde{V}\gamma$. Finally, using Eqs. (1) and (3), one obtains

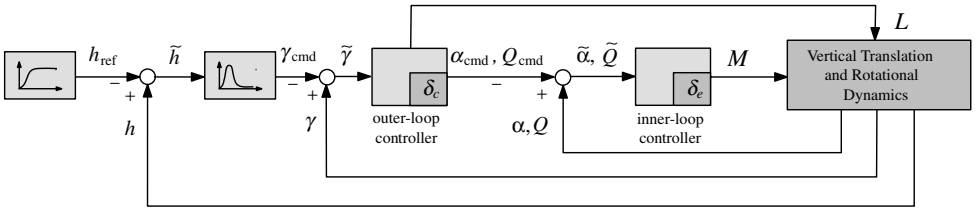

Fig. 2 Control of the vertical translation and rotational dynamics.

$$\dot{\tilde{\gamma}} = (1/mV)[\bar{q}SC_L^{\alpha}\alpha + T\sin\alpha - mg\cos\gamma + \bar{q}S(C_L^{\delta_e}\delta_e + C_L^{\delta_c}\delta_c + C_L^0 + \boldsymbol{C}_L^{\eta}\boldsymbol{\eta}) - mV\dot{\gamma}_{cmd}] \quad (7)$$

The first two terms on the right-hand side of Eq. (7) will be used to generate the stabilizing control α_{cmd}. Define the parameterized function of α

$$\Lambda(\alpha, \alpha^*, \bar{q}, \Phi) := \bar{q}SC_L^{\alpha}\alpha + T\sin\alpha - \bar{q}SC_L^{\alpha}\alpha^* - T^*\sin\alpha^*$$

where $T^* = \bar{q}S[C_{T,\Phi}(\alpha^*)\Phi + C_T(\alpha^*) + \boldsymbol{C}_T^{\eta}\boldsymbol{\eta}]$. Then the following "sector-boundedness" property can be established:

Property III.1: For all admissible values of $\alpha, \alpha^*, \bar{q}$, and Φ given in Table 1, the function $\Lambda(\alpha, \alpha^*, \bar{q}, \Phi)$ can be written as $\Lambda(\alpha, \alpha^*, \bar{q}, \Phi) = K_{\alpha_1}(\boldsymbol{x}, \Phi)V^2(\alpha - \alpha^*)$, where $K_{\alpha_1}(\boldsymbol{x}, \Phi)$ is a state-dependent coefficient satisfying $k_m \le K_{\alpha_1}(\boldsymbol{x}, \Phi) \le k_M$ for constants $k_m > 0$, $k_M > 0$.

Property III.1, sketched in Fig. 3a, is a consequence of the continuous differentiability of $\Lambda(\alpha, \alpha^*, \bar{q}, \Phi)$ with respect to its entries and can be verified graphically as follows. First, notice that because $\Lambda(\alpha^*, \alpha^*, \bar{q}, \Phi) = 0$, then $\Lambda(\alpha, \alpha^*, \bar{q}, \Phi) := K(\boldsymbol{x}, \Phi)(\alpha - \alpha^*)$, where $K(\boldsymbol{x}, \Phi)$ is a state-dependent coefficient. For any fixed α^* and $\bar{q}$ within their admissible ranges, the graph of the function $\Lambda(\alpha, \alpha^*, \bar{q}, \Phi)$ vs α can be bounded by two straight lines of

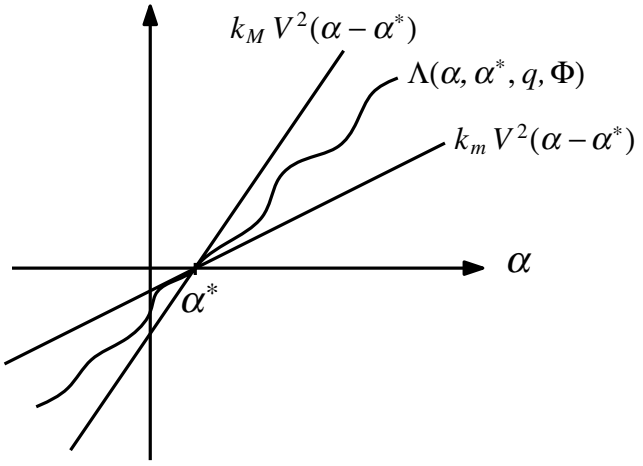

a) Bounds on $\Lambda(\alpha, \alpha^*, q, \Phi)$

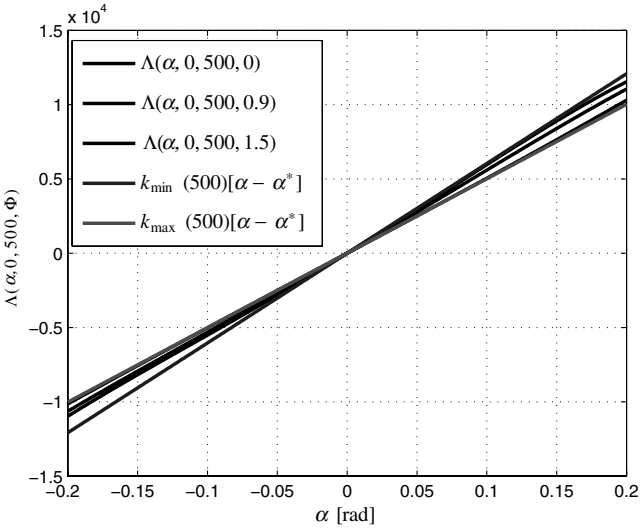

b) Bounds on $\Lambda(\alpha, 0, 500, \Phi)$

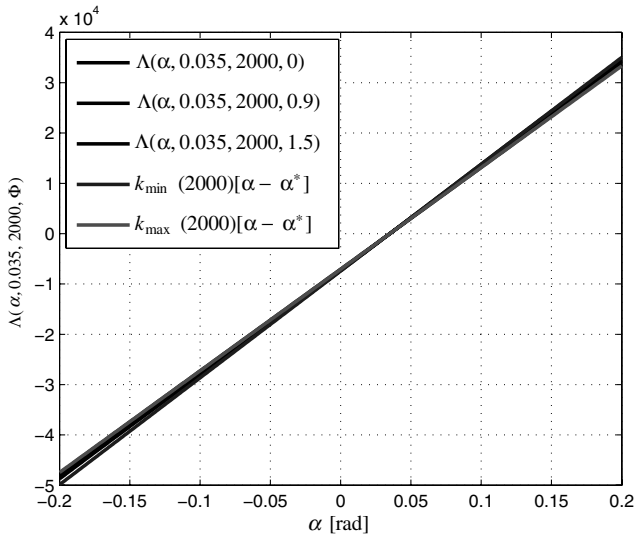

c) Bounds on $\Lambda(\alpha, 0.035, 2000, \Phi)$

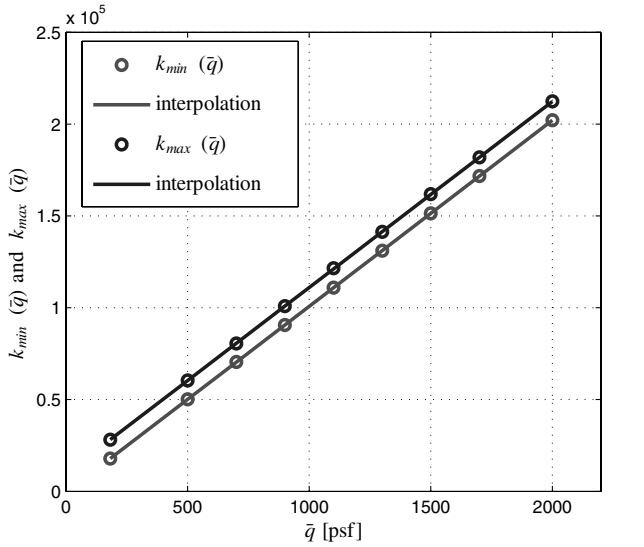

d) Bounds $k_{min}\,\bar{q}$ and $k_{max}\,\bar{q}$

Fig. 3 Sector-boundedness property of $\Lambda(\alpha, \alpha^*, \bar{q}_c, \Phi)$.

appropriate slope for any $\Phi \in \mathcal{A}$, that is, $k_{\min}(\bar{q}) < K(\boldsymbol{x}, \Phi) < k_{\max}(\bar{q})$ for two positive functions $k_{\min}(\bar{q})$ and $k_{\max}(\bar{q})$. Figures 3b and 3c show two such cases, corresponding to $\alpha^* = 0$ rad and $\bar{q} = 500$ psf and $\alpha^* = 0.035$ rad and $\bar{q} = 2000$ psf, respectively. Figure 3d shows the plot of $k_{\min}(\bar{q})$ and $k_{\max}(\bar{q})$ for selected values of $\bar{q}$; it is possible to see that these two functions can be approximated by two linear functions. As a result, for $\bar{q} \in \mathcal{A}$, there exist two positive constants $k_{\min}$ and $k_{\max}$ such that $k_{\min}\bar{q} < K(\boldsymbol{x}, \Phi) < k_{\max}\bar{q}$. Moreover, because $\bar{q} = 0.5\rho V^2$ and for the given range of altitude the air density satisfies the bound $0 < \rho_{\min} \leq \rho \leq \rho_{\max}$, it follows that in the range of flight conditions of interest the proposition holds for $K_{\alpha_1}(\boldsymbol{x}, \Phi) = K(\boldsymbol{x}, \Phi)/V^2$, $k_m := 0.5k_{\min}\rho_{\min}$, and $k_M := 0.5k_{\max}\rho_{\max}$.

The command trajectory for the angle of attack is selected as $\alpha_{\text{cmd}} = \alpha^* - \tilde{\gamma}$, as this choice yields a particularly simple form for the dynamics of the error $\tilde{\alpha}$. Because $\alpha = \alpha^* - \tilde{\gamma} + \tilde{\alpha}$, using property III.1, one obtains

$$\bar{q}SC_L^{\alpha}\alpha + T\sin\alpha = K_{\alpha_1}(\boldsymbol{x}, \Phi)V^2[\tilde{\alpha} - \tilde{\gamma}] + \bar{q}Sc_1(\alpha^*) + \bar{q}Sc_2(\alpha^*)\Phi + \bar{q}S\boldsymbol{C}_T^{\eta}\sin\alpha^*\tilde{\boldsymbol{\eta}}$$

where $c_1(\alpha^*) = C_T(\alpha^*)\sin\alpha^* + C_L^{\alpha}\alpha^* + \boldsymbol{C}_T^{\eta}\sin\alpha^*\boldsymbol{\eta}^*$ and $c_2(\alpha^*) = C_{T,\Phi}(\alpha^*)\sin\alpha^*$. Letting $\boldsymbol{\theta}_2$ and $\boldsymbol{\Psi}_2(\boldsymbol{x}, \boldsymbol{u}, \boldsymbol{y}_{\text{ref}})$ be defined, respectively, as

$$\boldsymbol{\theta}_2 = \left[\frac{C_L^{\delta_e}}{C_L^{\delta_c}}, \frac{C_L^0 + \boldsymbol{C}_L^{\eta}\boldsymbol{\eta}^* + c_1(\alpha^*)}{C_L^{\delta_c}}, \frac{c_2(\alpha^*)}{C_L^{\delta_c}}, \frac{m}{SC_L^{\delta_c}}\right]^T$$

$$\boldsymbol{\Psi}_2(\boldsymbol{x}, \boldsymbol{u}, \boldsymbol{y}_{\text{ref}}) = \left[-\delta_e, -1, -\Phi, \frac{1}{\bar{q}}(g\cos\gamma + V\dot{\gamma}_{\text{cmd}})\right]^T$$

the dynamics of $\tilde{\gamma}$ are written in the form

$$m\dot{\tilde{\gamma}} = K_{\alpha_1}(\boldsymbol{x}, \Phi)V[\tilde{\alpha} - \tilde{\gamma}] + \frac{\bar{q}SC_L^{\delta_c}}{V}[\delta_c - \boldsymbol{\Psi}_2(\boldsymbol{x}, \boldsymbol{u}, \boldsymbol{y}_{\text{ref}})^T\boldsymbol{\theta}_2] + \frac{\bar{q}S(\boldsymbol{C}_L^{\eta} + \boldsymbol{C}_T^{\eta}\sin\alpha^*)}{V}\tilde{\boldsymbol{\eta}} \tag{8}$$

Similar to the previous section, we denote with $\Theta_2 \subset \mathbb{R}^4$ the compact convex set obtained by letting the entries of $\boldsymbol{\theta}_2$ vary within the parameter set $\mathcal{P}$. Define the vector of estimates $\hat{\boldsymbol{\theta}}_2 \in \mathbb{R}^4$ and consider the control Lyapunov function candidate

$$W_2(\tilde{h}, \tilde{\gamma}, \tilde{\boldsymbol{\theta}}_2) = (\sigma_h/2)\tilde{h}^2 + (m/2)\tilde{\gamma}^2 + (SC_L^{\delta_c}/2)\tilde{\boldsymbol{\theta}}_2^T\Gamma_2^{-1}\tilde{\boldsymbol{\theta}}_2$$

where $\tilde{\boldsymbol{\theta}}_2 = \hat{\boldsymbol{\theta}}_2 - \boldsymbol{\theta}_2$, $\Gamma_2 \in \mathbb{R}^{4\times4}$ is a symmetric positive definite diagonal matrix, and $\sigma_h > 0$ is a scaling factor. The controller for the canard is given by the dynamical system

$$\dot{\hat{\boldsymbol{\theta}}}_2 = \text{Proj}_{\hat{\boldsymbol{\theta}}_2 \in \Theta_2}\left\{-\frac{\bar{q}\,\tilde{\gamma}}{V}\Gamma_2\boldsymbol{\Psi}_2(\boldsymbol{x}, \boldsymbol{u}, \boldsymbol{y}_{\text{ref}})\right\}$$
$$\delta_c = \boldsymbol{\Psi}_2(\boldsymbol{x}, \boldsymbol{u}, \boldsymbol{y}_{\text{ref}})^T\hat{\boldsymbol{\theta}}_2 - k_3\tilde{\gamma} \tag{9}$$

with initial conditions $\hat{\boldsymbol{\theta}}_2(0) \in \Theta_2$ and gain parameter $k_3 > 0$.

3. *Controller for the* (α, Q) *Subsystem*

The final steps in our design are to regulate $\tilde{\alpha}(t)$ to zero asymptotically and provide a comprehensive stability proof for the interconnected system. From the dynamics of $\tilde{\alpha}$, it is apparent that the command trajectory for the pitch rate should be selected as $Q_{\text{cmd}} = \dot{\gamma}_{\text{cmd}} - k_4\tilde{\alpha}$, with $k_4 > 0$. Using Eqs. (2) and (3), the error dynamics can be written as

$$\dot{\tilde{\alpha}} = -k_4\tilde{\alpha} + \tilde{Q}$$
$$\dot{\tilde{Q}} = \boldsymbol{\theta}_3^T[\boldsymbol{B}_3(\boldsymbol{x})\delta_e - \boldsymbol{\Psi}_3(\boldsymbol{x}, \boldsymbol{u}, \boldsymbol{y}_{\text{ref}})] + k_4\tilde{Q} - k_4^2\tilde{\alpha} + \frac{\bar{q}S}{I_{yy}}[z_T\boldsymbol{C}_T^{\eta} + \bar{c}\boldsymbol{C}_M^{\eta}]\tilde{\boldsymbol{\eta}} \tag{10}$$

where the vector of uncertain parameters $\boldsymbol{\theta}_3 \in \mathbb{R}^{11}$, the regressor $\boldsymbol{\Psi}_3(\boldsymbol{x}, \boldsymbol{u}, \boldsymbol{y}_{\text{ref}})$, and the input matrix $\boldsymbol{B}_3(\boldsymbol{x})$ are given, respectively, by

$$\boldsymbol{\theta}_3 = (S/I_{yy})[\bar{c}C_M^{\delta_e}, \bar{c}C_M^{\delta_c}, z_TC_T^{\Phi\alpha^3}, z_TC_T^{\Phi\alpha^2}, z_TC_T^{\Phi\alpha}, z_TC_T^{\Phi}, z_TC_T^3, (z_TC_T^2 + \bar{c}C_M^{\alpha^2}), (z_TC_T^1 + \bar{c}C_M^{\alpha}), (z_TC_T^0 + \bar{c}C_M^0) + (z_T\boldsymbol{C}_T^{\eta} + \bar{c}\boldsymbol{C}_M^{\eta})\boldsymbol{\eta}^*, I_{yy}/S]^T$$

$$\boldsymbol{\Psi}_3(\boldsymbol{x}, \boldsymbol{u}, \boldsymbol{y}_{\text{ref}}) = -\bar{q}[0, \delta_c, \alpha^3\Phi, \alpha^2\Phi, \alpha\Phi, \Phi, \alpha^3, \alpha^2, \alpha, 1, -\ddot{\gamma}_{\text{cmd}}/\bar{q}]^T$$

$$\boldsymbol{B}_3(\boldsymbol{x}) = [\bar{q}, \boldsymbol{0}_{1\times10}]^T$$

Finally, denote by $\Theta_3 \subset \mathbb{R}^{11}$ the convex and compact parameter set for $\boldsymbol{\theta}_3$ and define the estimate vector $\hat{\boldsymbol{\theta}}_3$ and the error $\tilde{\boldsymbol{\theta}}_3 = \hat{\boldsymbol{\theta}}_3 - \boldsymbol{\theta}_3$. The design is completed by selecting

$$W_3(\tilde{\alpha}, \tilde{Q}, \tilde{\boldsymbol{\theta}}_3) = (\sigma_{\alpha}/2)\tilde{\alpha}^2 + (\sigma_Q/2)\tilde{Q}^2 + (\sigma_Q/2)\tilde{\boldsymbol{\theta}}_3^T\Gamma_3^{-1}\tilde{\boldsymbol{\theta}}_3$$

with scaling factors $\sigma_{\alpha} > 0$, $\sigma_Q > 0$, and positive definite $\Gamma_3 \in \mathbb{R}^{11\times11}$, yielding the controller

$$\dot{\hat{\boldsymbol{\theta}}}_3 = \text{Proj}_{\boldsymbol{\theta}_3 \in \Theta_3}\{\Gamma_3[\boldsymbol{B}_3(\boldsymbol{x})\delta_e - \boldsymbol{\Psi}_3(\boldsymbol{x}, \boldsymbol{u}, \boldsymbol{y}_{\text{ref}})]\tilde{Q}\}$$
$$\delta_e = \frac{1}{\hat{\boldsymbol{\theta}}_3^T\boldsymbol{B}_3(\boldsymbol{x})}[\boldsymbol{\Psi}_3(\boldsymbol{x}, \boldsymbol{u}, \boldsymbol{y}_{\text{ref}})^T\hat{\boldsymbol{\theta}}_3 - k_5\tilde{Q}] \tag{11}$$

where $\hat{\boldsymbol{\theta}}_3(0) \in \Theta_3$ and $k_5 > 0$ is a gain parameter.

4. *Stability Analysis for the Rigid-Body Dynamics*

To prove stability of the overall closed-loop system obtained by interconnecting the rigid-body dynamics in Eqs. (1) and (2) with the adaptive controller given by Eqs. (6), (9), and (11), consider the Lyapunov function candidate

$$W_{\text{rb}}(\tilde{\boldsymbol{x}}, \tilde{\boldsymbol{\theta}}) = W_1(\tilde{V}, \tilde{\boldsymbol{\theta}}_1) + W_2(\tilde{h}, \tilde{\gamma}, \tilde{\boldsymbol{\theta}}_2) + W_3(\tilde{\alpha}, \tilde{Q}, \tilde{\boldsymbol{\theta}}_3) \tag{12}$$

where $\tilde{\boldsymbol{\theta}} = [\tilde{\boldsymbol{\theta}}_1^T, \tilde{\boldsymbol{\theta}}_2^T, \tilde{\boldsymbol{\theta}}_3^T]^T$. The role of the scaling factors in the Lyapunov function $W_{\text{rb}}(\tilde{\boldsymbol{x}}, \tilde{\boldsymbol{\theta}})$ is to allow flexibility in the design by shaping the level sets $\Omega_c(W_{\text{rb}}) = \{\tilde{\boldsymbol{x}}, \tilde{\boldsymbol{\theta}} | W_{\text{rb}}(\tilde{\boldsymbol{x}}, \tilde{\boldsymbol{\theta}}) \leq c\}$, $c > 0$, to obtain the required estimate of the domain of attraction. In particular, given the compact set $\Xi_0^{\tilde{x}}$ of initial conditions and the parameter set $\Theta = \Theta_1 \times \Theta_2 \times \Theta_3$, it is always possible to determine a constant $c > 0$ and values of the scaling factors σ_{χ}, σ_V, σ_h, σ_{α}, and σ_Q such that, for a given reference, $\boldsymbol{y}_{\text{ref}}$, the following conditions are verified for all $\boldsymbol{p} \in \mathcal{P}$:

a1) $\Xi_0^{\tilde{x}} \subset \Omega_c(W_{\text{rb}})$;
a2) $\tilde{\boldsymbol{x}} \in \Omega_c(W_{\text{rb}})$ implies $\boldsymbol{x} \in \mathcal{A}$;
a3) $\hat{\boldsymbol{\theta}}$, $\boldsymbol{\theta} \in \Theta$ implies $\tilde{\boldsymbol{\theta}} \in \Omega_c(W_{\text{rb}})$.

The first two conditions ensure that the domain of attraction of the equilibrium set at $\tilde{\boldsymbol{x}} = 0$ includes the given compact set $\Xi_0^{\tilde{x}}$ and that the trajectory $\boldsymbol{x}(t)$ remains within the feasible set, $\mathcal{A}$, if the derivative of the Lyapunov function is negative semidefinite on $\Omega_c(W_{\text{rb}})$. The third condition implies that the estimates $\hat{\boldsymbol{\theta}}(t)$, when projected onto the set Θ, generate an error that remains within the level set $\Omega_c(W_{\text{rb}})$.

Proposition III.1 Consider the closed-loop system

$$m\dot{\tilde{V}} = -k_1\tilde{V} - [\boldsymbol{B}_1(\boldsymbol{x})^T\Phi - \boldsymbol{\Psi}_1(\boldsymbol{x}, \boldsymbol{u}, \boldsymbol{y}_{\text{ref}})^T]\tilde{\boldsymbol{\theta}}_1 + \bar{q}S[\boldsymbol{C}_T^{\eta}\cos\alpha - \boldsymbol{C}_D^{\eta}]\tilde{\boldsymbol{\eta}}$$
$$\dot{\tilde{h}} = -k_2V_{\text{ref}}\tilde{h} + V_{\text{ref}}\tilde{\gamma} + \tilde{V}\gamma$$
$$m\dot{\tilde{\gamma}} = K_{\alpha_1}(\boldsymbol{x}, \Phi)V[\tilde{\alpha} - \tilde{\gamma}] + \frac{\bar{q}SC_L^{\delta_c}}{V}[-k_3\tilde{\gamma} + \boldsymbol{\Psi}_2(\boldsymbol{x}, \boldsymbol{u}, \boldsymbol{y}_{\text{ref}})^T\tilde{\boldsymbol{\theta}}_2] + \frac{\bar{q}S(\boldsymbol{C}_L^{\eta} + \boldsymbol{C}_T^{\eta}\sin\alpha^*)}{V}\tilde{\boldsymbol{\eta}}$$
$$\dot{\tilde{\alpha}} = -k_4\tilde{\alpha} + \tilde{Q}$$
$$\dot{\tilde{Q}} = -(k_5 - k_4)\tilde{Q} - k_4^2\tilde{\alpha} - [\boldsymbol{B}_3(\boldsymbol{x})^T\delta_e - \boldsymbol{\Psi}_3(\boldsymbol{x}, \boldsymbol{u}, \boldsymbol{y}_{\text{ref}})^T]\tilde{\boldsymbol{\theta}}_3 + \frac{\bar{q}S}{I_{yy}}[z_T\boldsymbol{C}_T^{\eta} + \bar{c}\boldsymbol{C}_M^{\eta}]\tilde{\boldsymbol{\eta}}$$
$$\dot{\hat{\boldsymbol{\theta}}}_1 = \text{Proj}_{\hat{\boldsymbol{\theta}}_1 \in \Theta_1}\{\tilde{V}\Gamma_1[\boldsymbol{B}_1(\boldsymbol{x})\Phi - \boldsymbol{\Psi}_1(\boldsymbol{x}, \boldsymbol{u}, \boldsymbol{y}_{\text{ref}})]\}$$

$$\dot{\hat{\boldsymbol{\theta}}}_2 = \mathrm{Proj}_{\hat{\boldsymbol{\theta}}_2 \in \Theta_2}\left\{-\frac{\bar{q}\,\tilde{\gamma}}{V}\Gamma_2 \boldsymbol{\Psi}_2(\boldsymbol{x}, \boldsymbol{u}, \boldsymbol{y}_{\mathrm{ref}})\right\}$$

$$\dot{\hat{\boldsymbol{\theta}}}_3 = \mathrm{Proj}_{\hat{\boldsymbol{\theta}}_3 \in \Theta_3}\{\Gamma_3[\boldsymbol{B}_3(\boldsymbol{x})\delta_e - \boldsymbol{\Psi}_3(\boldsymbol{x}, \boldsymbol{u}, \boldsymbol{y}_{\mathrm{ref}})]\tilde{Q}\} \tag{13}$$

and the Lyapunov function candidate given in Eq. (12). Let the level set $\Omega_c(W_{\mathrm{rb}})$ be chosen to satisfy conditions a1–a3. Fix, arbitrarily, the value of the gains $k_1 > 0$ and $k_3 \geq 0$. Then, there exist positive numbers $k_i^\star$, $i = 2, 4, 5$, such that, if $\tilde{\eta} = 0$, the trajectories of the closed-loop system (13) originating within $\Omega_c(W_{\mathrm{rb}})$ are bounded and satisfy $\lim_{t\to\infty} \tilde{\boldsymbol{x}}(t) = 0$ whenever the remaining gains are selected to satisfy $k_i > k_i^\star$, $i = 2, 4, 5$.

Proof. Using standard properties of the projection operator [31] and condition a3, it can be verified that the derivative of W_{rb} along the trajectories of system (13) satisfies

$$\dot{W}_{\mathrm{rb}}(\tilde{\boldsymbol{x}}, \tilde{\boldsymbol{\theta}}) \leq -\tilde{\boldsymbol{x}}^T \boldsymbol{R}_{\mathrm{rb}}(\boldsymbol{x}, \boldsymbol{y}_{\mathrm{ref}})\tilde{\boldsymbol{x}} + \tilde{\boldsymbol{x}}^T \boldsymbol{R}_{\mathrm{rb,fl}}(\boldsymbol{x})\tilde{\boldsymbol{\eta}} \quad \forall\ (\tilde{\boldsymbol{x}}, \tilde{\boldsymbol{\theta}}) \in \Omega_c(W_{\mathrm{rb}}) \tag{14}$$

where $\boldsymbol{R}_{\mathrm{rb}}(\boldsymbol{x}, \boldsymbol{y}_{\mathrm{ref}})$ is the state-dependent matrix

$$\boldsymbol{R}_{\mathrm{rb}}(\boldsymbol{x}, \boldsymbol{y}_{\mathrm{ref}}) := \begin{bmatrix} k_1\sigma_V & -\frac{\sigma_h\gamma}{2} & 0 & 0 & 0 \\ -\frac{\sigma_h\gamma}{2} & \sigma_h k_2 V_{\mathrm{ref}} & -\frac{\sigma_h V_{\mathrm{ref}}}{2} & 0 & 0 \\ 0 & -\frac{\sigma_h V_{\mathrm{ref}}}{2} & (K_{\alpha_1} + \frac{\bar{q}SC_L^{\delta_c}}{V^2}k_3)V & -\frac{K_{\alpha_1}V}{2} & 0 \\ 0 & 0 & -\frac{K_{\alpha_1}V}{2} & \sigma_\alpha k_4 & \frac{\sigma_Q k_4^2 - \sigma_\alpha}{2} \\ 0 & 0 & 0 & \frac{\sigma_Q k_4^2 - \sigma_\alpha}{2} & \sigma_Q(k_5 - k_4) \end{bmatrix}$$

and the matrix

$$\boldsymbol{R}_{\mathrm{rb,fl}}(x) := \bar{q}S\begin{bmatrix} \sigma_V(\boldsymbol{C}_T^\eta \cos\alpha - \boldsymbol{C}_D^\eta) \\ 0_{1\times 6} \\ \frac{\boldsymbol{C}_L^\eta + \boldsymbol{C}_T^\eta \sin\alpha^*}{V} \\ 0_{1\times 6} \\ \sigma_Q \frac{z_T \boldsymbol{C}_T^\eta + \bar{c}\boldsymbol{C}_M^\eta}{I_{yy}} \end{bmatrix} \in \mathbb{R}^{5\times 6}$$

determines the coupling between the rigid-body tracking error and the structural flexibility. Using conditions a1–a2, the lower bound in property III.1, and the fact that $C_L^{\delta_c} > 0$, it is seen that for any $\tilde{\boldsymbol{x}} \in \Omega_c(W_{\mathrm{rb}})$ the (3,3) element of $\boldsymbol{R}_{\mathrm{rb}}$ satisfies

$$K_{\alpha_1} + \frac{\bar{q}SC_L^{\delta_c}}{V^2}k_3 \geq k_m + k_c k_3, \qquad k_c := \min_{\substack{V,\tilde{q}\in\mathcal{A} \\ p\in\mathcal{P}}} \frac{\bar{q}SC_L^{\delta_c}}{V^2} > 0$$

Fix $k_3 \geq 0$, and let Δ_i denote the ith minor of $\boldsymbol{R}_{\mathrm{rb}}(\boldsymbol{x}, \boldsymbol{y}_{\mathrm{ref}})$. For any $k_1 > 0$, the number

$$k_2^\star := \frac{\sigma_h}{4\sigma_V k_1 \min_{V_{\mathrm{ref}}\in\mathcal{A}} V_{\mathrm{ref}}} + \frac{\sigma_h \max_{V_{\mathrm{ref}}\in\mathcal{A}} V_{\mathrm{ref}}}{4(k_m + k_c k_3)\min_{V\in A} V}$$

is such that the minors Δ_1, Δ_2, and Δ_3 are strictly positive for any $k_2 > k_2^*$. Because Δ_1, Δ_2, and Δ_3 do not depend on k_4, there exists $k_4^\star$ (which depends on k_1, k_2, and k_3) such that Δ_4 is positive for any $k_4 > k_4^\star$. Similarly, there exists $k_5^\star$ such that Δ_5 is positive for all $k_5 > k_5^\star$. By Sylvester's criterion it follows that there exists a constant symmetric positive definite matrix $\bar{\boldsymbol{R}}_{\mathrm{rb}}$ such that $\boldsymbol{R}_{\mathrm{rb}}(\boldsymbol{x}, \boldsymbol{y}_{\mathrm{ref}}) \geq \bar{\boldsymbol{R}}_{\mathrm{rb}}$. As a result, for all $(\tilde{\boldsymbol{x}}, \tilde{\boldsymbol{\theta}}) \in \Omega_c(W_{\mathrm{rb}})$ and $\tilde{\boldsymbol{\eta}} = 0$

$$\dot{W}_{\mathrm{rb}}(\tilde{\boldsymbol{x}}, \tilde{\boldsymbol{\theta}}) \leq -\tilde{\boldsymbol{x}}^T \bar{\boldsymbol{R}}_{\mathrm{rb}} \tilde{\boldsymbol{x}}$$

Thus, the result follows from the application of LaSalle–Yoshizawa theorem [31,34]. □

Notice that a nonzero value of k_3 is not needed for stability of the rigid-body closed-loop system and that k_1 can be chosen arbitrarily. Once k_1 and k_3 have been fixed, the minimal values of the other gains that ensure closed-loop stability can be determined, and any number larger than these values can be selected for the gains. This result is in sharp contrast with the outcome of the analysis when the structural dynamics are taken into consideration.

IV. Stability Analysis of the Rigid-Body and Flexible Dynamics

Because the system has vector relative degree [35] $r = [1, 2, 2]^T$ with respect to the output $[V, h, \alpha]^T$, the CDM possesses six-dimensional internal dynamics, related to the structural dynamics. To compute the internal dynamics, we begin by substituting the generalized forces N_i in Eq. (2) into the last equation of Eq. (1), obtaining

$$\dot{\boldsymbol{\eta}} = \boldsymbol{A}_\eta \boldsymbol{\eta} + \bar{q}S[\boldsymbol{A}_1\alpha + \boldsymbol{A}_2\alpha^2 + \boldsymbol{A}_3] + \bar{q}S\boldsymbol{A}_4\boldsymbol{\delta} \tag{15}$$

where

$$\boldsymbol{A}_\eta = \begin{bmatrix} 0 & 1 & 0 & 0 & 0 & 0 \\ -\omega_1^2 + \bar{q}SN_1^{\eta_1} & -2\zeta_1\omega_1 & \bar{q}SN_1^{\eta_2} & 0 & \bar{q}SN_1^{\eta_3} & 0 \\ 0 & 0 & 0 & 1 & 0 & 0 \\ \bar{q}SN_2^{\eta_1} & 0 & -\omega_2^2 + \bar{q}SN_2^{\eta_2} & -2\zeta_2\omega_2 & \bar{q}SN_2^{\eta_3} & 0 \\ 0 & 0 & 0 & 0 & 0 & 1 \\ \bar{q}SN_3^{\eta_1} & 0 & \bar{q}SN_3^{\eta_2} & 0 & -\omega_3^2 + \bar{q}SN_3^{\eta_3} & -2\zeta_3\omega_3 \end{bmatrix}$$

$$\boldsymbol{A}_1 = [0 \quad N_1^\alpha \quad 0 \quad N_2^\alpha \quad 0 \quad N_3^\alpha]^T, \qquad \boldsymbol{A}_2 = [0 \quad N_1^{\alpha^2} \quad 0 \quad N_2^{\alpha^2} \quad 0 \quad N_3^{\alpha^2}]^T$$

$$\boldsymbol{A}_3 = [0 \quad N_1^0 \quad 0 \quad N_2^0 \quad 0 \quad N_3^0]^T, \qquad \boldsymbol{A}_4 = \begin{bmatrix} 0 & N_1^{\delta_c} & 0 & N_2^{\delta_c} & 0 & N_3^{\delta_c} \\ 0 & N_1^{\delta_e} & 0 & N_2^{\delta_e} & 0 & N_3^{\delta_e} \end{bmatrix}^T$$

Next, we remove the dependence of Eq. (15) on the control inputs. Using the same arguments used in property III.1, one can express the term $\bar{q}SC_L^{\alpha}\alpha + T\sin\alpha$ appearing in the dynamic equation of the angle of attack as $\bar{q}SC_L^{\alpha}\alpha + T\sin\alpha = \bar{q}SK_{\alpha_2}(\boldsymbol{x},\Phi)\alpha$, where the coefficient $K_{\alpha_2}(\boldsymbol{x},\Phi)$ is bounded in the feasible set $\mathcal{A}$. As a result, using Eqs. (3), the (α, Q) dynamics can be written as

$$\begin{bmatrix}\dot{\alpha}\\ \dot{Q}\end{bmatrix} = \bar{q}S\boldsymbol{G}_1(V)\boldsymbol{\delta} + \boldsymbol{G}_2(\boldsymbol{x})\boldsymbol{\eta} + \boldsymbol{G}_3(\boldsymbol{x},\boldsymbol{u}) \tag{16}$$

where

$$\boldsymbol{G}_1(V) = \begin{bmatrix} -\frac{C_L^{\delta_c}}{mV} & -\frac{C_L^{\delta_e}}{mV}\\ \frac{\bar{c}C_M^{\delta_c}}{I_{yy}} & \frac{\bar{c}C_M^{\delta_e}}{I_{yy}}\end{bmatrix}$$

$$\boldsymbol{G}_2(x) = \bar{q}S\begin{bmatrix} -\frac{C_L^{\eta_1}}{mV} & 0 & -\frac{C_L^{\eta_2}}{mV} & 0 & -\frac{C_L^{\eta_3}}{mV} & 0\\ \frac{\bar{c}C_M^{\eta_1}}{I_{yy}} & 0 & \frac{\bar{c}C_M^{\eta_2}}{I_{yy}} & 0 & \frac{\bar{c}C_M^{\eta_3}}{I_{yy}} & 0\end{bmatrix}$$

$$\boldsymbol{G}_3(\boldsymbol{x},\boldsymbol{u}) = \begin{bmatrix} -\frac{\bar{q}S}{mV}(K_{\alpha_2}(x,\Phi)\alpha + C_L^0) + Q + \frac{g}{V}\cos\gamma\\ \frac{\bar{q}S\bar{c}}{I_{yy}}(C_M^{\alpha^2}\alpha^2 + C_M^{\alpha}\alpha + C_M^0) + \frac{z_T}{I_{yy}}T\end{bmatrix}$$

The change of coordinates

$$\boldsymbol{\chi} = \boldsymbol{\eta} - \boldsymbol{B}_X\boldsymbol{G}_1^{-1}(V_{\text{ref}})\begin{bmatrix}\alpha\\ Q\end{bmatrix} + \frac{m}{\cos\alpha^*}\boldsymbol{D}_X\tilde{V} \tag{17}$$

will be applied to Eq. (15), where

$$\boldsymbol{B}_X = \begin{bmatrix} 0 & B_{X_{11}} & 0 & B_{X_{21}} & 0 & B_{X_{31}}\\ 0 & B_{X_{12}} & 0 & B_{X_{22}} & 0 & B_{X_{32}}\end{bmatrix}^T$$

$$\boldsymbol{D}_X = [\,0 \quad D_{X_1} \quad 0 \quad D_{X_2} \quad 0 \quad D_{X_3}\,]^T$$

are constant matrices to be determined. In particular, $\boldsymbol{B}_X$ will be chosen to remove the explicit dependence of the flexible states on the aerodynamic control surfaces, whereas $\boldsymbol{D}_X$ will be selected to suppress the term that depends on thrust (hence, on Φ) that appears in the χ dynamics by way of the second addendum of Eq. (17). The special structure of the matrix $\boldsymbol{A}_4$ dictates the selected structure of the matrices $\boldsymbol{B}_X$ and $\boldsymbol{D}_X$. Because the transformation (17) modifies only the time derivative of the flexible modes, it follows that $\chi_{2i-1} = \eta_i$, $i = 1, 2, 3$. This useful property will be exploited later in the section, when the interconnection with the rigid-body dynamics is considered.

Using Eqs. (1–3), the χ dynamics are written as

$$\begin{aligned}\dot{\boldsymbol{\chi}} = {} & \left[\boldsymbol{A}_\eta - \boldsymbol{B}_X\boldsymbol{G}_1^{-1}(V_{\text{ref}})\boldsymbol{G}_2(\boldsymbol{x}) - \frac{\bar{q}S}{\cos\alpha^*}\boldsymbol{D}_X\boldsymbol{C}_D^{\eta}\right]\boldsymbol{\chi}\\ & + \left[\boldsymbol{A}_\eta\boldsymbol{B}_X\boldsymbol{G}_1^{-1}(V_{\text{ref}}) - \boldsymbol{B}_X\frac{\partial\boldsymbol{G}_1^{-1}}{\partial V_{\text{ref}}}\dot{V}_{\text{ref}}\right]\begin{bmatrix}\alpha\\ Q\end{bmatrix} - \frac{m\boldsymbol{A}_\eta\boldsymbol{D}_X}{\cos\alpha^*}\tilde{V}\\ & + \bar{q}S\left[\left(\boldsymbol{A}_1 - \frac{C_D^{\alpha}\boldsymbol{D}_X}{\cos\alpha^*}\right)\alpha + \left(\boldsymbol{A}_2 - \frac{C_D^{\alpha^2}\boldsymbol{D}_X}{\cos\alpha^*}\right)\alpha^2\right.\\ & \left. + \left(\boldsymbol{A}_3 - \frac{C_D^0\boldsymbol{D}_X}{\cos\alpha^*}\right)\right] + \bar{q}S\left[[\boldsymbol{A}_4 - \boldsymbol{B}_X\boldsymbol{G}_1^{-1}(V_{\text{ref}})\boldsymbol{G}_1(V)]\boldsymbol{\delta}\right.\\ & \left. - \frac{\boldsymbol{D}_X}{\cos\alpha^*}(C_D^{\delta_e^2}\delta_e^2 + C_D^{\delta_e}\delta_e + C_D^{\delta_c^2}\delta_c^2 + C_D^{\delta_c}\delta_c)\right]\\ & - \frac{mg\sin\gamma}{\cos\alpha^*}\boldsymbol{D}_X - \frac{m\boldsymbol{D}_X}{\cos\alpha^*}\dot{V}_{\text{ref}} - \boldsymbol{B}_X\boldsymbol{G}_1^{-1}(V_{\text{ref}})\boldsymbol{G}_3(\boldsymbol{x},\boldsymbol{u})\\ & + \frac{\cos\alpha}{\cos\alpha^*}\boldsymbol{D}_X T\end{aligned} \tag{18}$$

Note that only the last two terms in Eq. (18) depend on T. Defining

$$\begin{aligned} N_i^{M\delta} &:= C_M^{\delta_e}B_{X_{i1}} - C_M^{\delta_c}B_{X_{i2}}\\ N_i^{L\delta} &:= C_L^{\delta_e}B_{X_{i1}} - C_L^{\delta_c}B_{X_{i2}}, \quad i = 1,2,3\\ C_A &:= \frac{1}{C_M^{\delta_c}C_L^{\delta_e} - C_L^{\delta_c}C_M^{\delta_e}}, \qquad C_B := \frac{C_A z_T}{\bar{c}\cos\alpha^*}\end{aligned}$$

and using the assumption $\cos\alpha \approx \cos\alpha^*$, which is valid within the bounds given in Table 1, it is seen that the choice

$$\boldsymbol{D}_X = (C_A z_T/\bar{c})[\,0 \quad N_1^{L\delta} \quad 0 \quad N_2^{L\delta} \quad 0 \quad N_3^{L\delta}\,]^T$$

removes the occurrence of T in Eq. (18). The terms in Eq. (18) that depend on $\boldsymbol{\delta}$, that is,

$$\begin{aligned}&[\boldsymbol{A}_4 - \boldsymbol{B}_X\boldsymbol{G}_1^{-1}(V_{\text{ref}})\boldsymbol{G}_1(V)]\boldsymbol{\delta} - (\boldsymbol{D}_X/\cos\alpha^*)\\ &\quad\times[C_D^{\delta_e^2}\delta_e^2 + C_D^{\delta_e}\delta_e + C_D^{\delta_c^2}\delta_c^2 + C_D^{\delta_c}\delta_c]\end{aligned}$$

can be gathered into the vector

$$\begin{aligned}&\boldsymbol{C}^{\boldsymbol{\delta}}(\delta_c,\delta_e,\bar{V})\\ &\quad = [\,0 \quad C_1^{\delta}(\delta_c,\delta_e,\bar{V}) \quad 0 \quad C_2^{\delta}(\delta_c,\delta_e,\bar{V}) \quad 0 \quad C_3^{\delta}(\delta_c,\delta_e,\bar{V})\,]^T\end{aligned}$$

where $\bar{V} := \tilde{V}/V$, and

$$\begin{aligned}C_i^{\delta}(\delta_c,\delta_e,\bar{V}) = {} & N_i^{\delta_c}\delta_c + N_i^{\delta_e}\delta_e\\ & - C_B N_i^{L\delta}[C_D^{\delta_e^2}\delta_e^2 + C_D^{\delta_e}\delta_e + C_D^{\delta_c^2}\delta_c^2 + C_D^{\delta_c}\delta_c] - B_{Xi1}\delta_c - B_{Xi2}\delta_e\\ & - C_A N_i^{M\delta}(C_L^{\delta_c}\delta_c + C_L^{\delta_e}\delta_e)\bar{V} \qquad i = 1,2,3\end{aligned}$$

The task is now to determine $\boldsymbol{B}_X$ so that the functions C_i^{δ} are identically zero. Because of the quadratic dependence of C_i^{δ} on $\boldsymbol{\delta}$ and the presence of the term $\bar{V}$, it is not possible to completely eliminate the input $\boldsymbol{\delta}$ from the χ dynamics using a change of coordinates. Notice that, had $\boldsymbol{G}_1^{-1}(V)$ been considered in place of $\boldsymbol{G}_1^{-1}(V_{\text{ref}})$ in Eq. (17), the terms multiplied by $\bar{V}$ in C_i^{δ} would have vanished. However, the time derivative of V would appear instead of $\dot{V}_{\text{ref}}$ in Eq. (18), and the complexity of the transformed system would have significantly increased. As a compromise, the change of coordinate (17) has been adopted, with the coefficients of the matrix $\boldsymbol{B}_X$ selected as the solution to the following optimization problem:

$$\begin{aligned}(B_{X_{i1}}, B_{X_{i2}}) = \arg\min_{(B_{X_{i1}},B_{X_{i2}})}\frac{1}{N}\sum_{k=1}^{N}\left[\int_{\delta_{c_{\min}}}^{\delta_{c_{\max}}}|C_i^{\delta}(\delta_c,0,\bar{V}_k)|\,\mathrm{d}\delta_c\right.\\ \left. + \int_{\delta_{e_{\min}}}^{\delta_{e_{\max}}}|C_i^{\delta}(0,\delta_e,\bar{V}_k)|\,\mathrm{d}\delta_e\right]\end{aligned}$$

where $\bar{V}$ is evaluated on a grid $\{\bar{V}_k\}_{k=1}^N$ of feasible values. Although this choice for $B_{X_{i1}}$ and $B_{X_{i2}}$ does not render the functions C_i^{δ} identically zero, the effect of the aerodynamic control surfaces on the flexible states is significantly reduced so that the terms C_i^{δ} can be neglected. This is confirmed by the plots in Fig. 4, which show a comparison between the influence of the input $\boldsymbol{\delta}$ on the generalized elastic forces before and after the change of coordinates. Letting $\sin\gamma \approx \gamma$, the change of coordinates (17) transforms Eq. (18) into

$$\dot{\boldsymbol{\chi}} = (\boldsymbol{A}_{\text{st}} + \boldsymbol{A}_p)\boldsymbol{\chi} + \boldsymbol{J}_0 + \boldsymbol{J}_1\alpha + \boldsymbol{J}_2\alpha^2 + \boldsymbol{J}_3 Q + \boldsymbol{J}_4\tilde{V} + \boldsymbol{J}_5\gamma \tag{19}$$

where the vectors $\boldsymbol{J}_i$, $0 \le i \le 5$, are given in the Appendix, the matrices $\boldsymbol{A}_{\text{st}}$ and $\boldsymbol{A}_p$ are

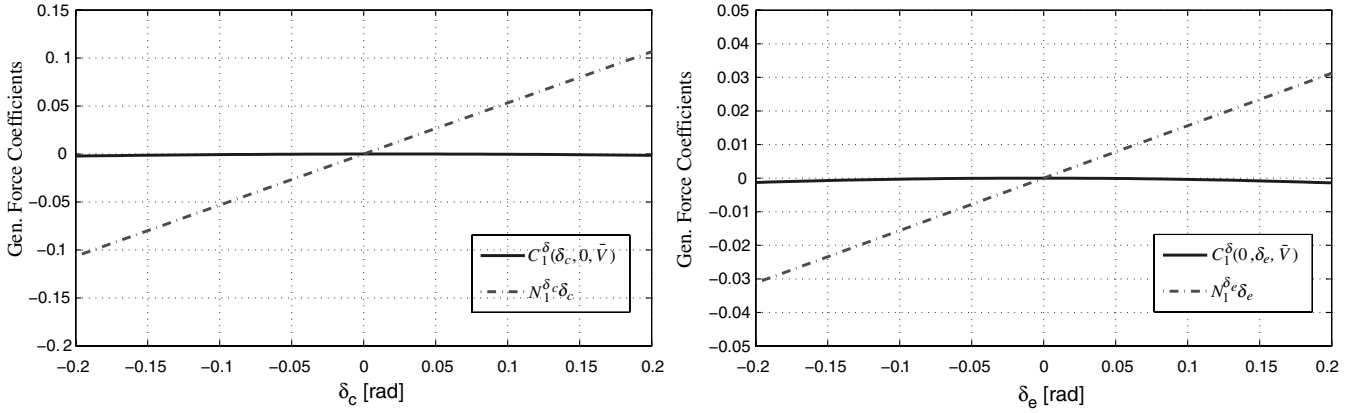

a) Comparison between $N_1^{\delta_c}\delta_c$ and $C_1^{\delta}(\delta_c, 0, \bar{V})$ **b) Comparison between $N_1^{\delta_e}\delta_e$ and $C_1^{\delta}(0, \delta_e, \bar{V})$**

Fig. 4 Influence of the control surfaces on the original flexible dynamics and after the change of coordinates. In the plots, the representative value $\bar{V} = 6 \times 10^{-3}$ has been selected.

$$\boldsymbol{A}_{\text{st}} = \begin{bmatrix} 0 & 1 & 0 & 0 & 0 & 0 \\ -\omega_1^2 & -2\zeta_1\omega_1 & 0 & 0 & 0 & 0 \\ 0 & 0 & 0 & 1 & 0 & 0 \\ 0 & 0 & -\omega_2^2 & -2\zeta_2\omega_2 & 0 & 0 \\ 0 & 0 & 0 & 0 & 0 & 1 \\ 0 & 0 & 0 & 0 & -\omega_3^2 & -2\zeta_3\omega_3 \end{bmatrix}$$

$$\boldsymbol{A}_p = \begin{bmatrix} 0 & 0 & 0 & 0 & 0 & 0 \\ P_{11} & 0 & P_{12} & 0 & P_{13} & 0 \\ 0 & 0 & 0 & 0 & 0 & 0 \\ P_{21} & 0 & P_{22} & 0 & P_{23} & 0 \\ 0 & 0 & 0 & 0 & 0 & 0 \\ P_{31} & 0 & P_{32} & 0 & P_{33} & 0 \end{bmatrix}$$

and

$$P_{jk} = \bar{q}S[N_j^{\eta_k} + C_A(N_j^{M\delta}C_L^{\eta_k}V_{\text{ref}}/V - N_j^{L\delta}C_M^{\eta_k}) - C_B N_j^{L\delta}C_D^{\eta_k}]$$
$$1 \le j, k \le 3$$

Because the damping ratios, ζ_i, are positive, the matrix $\boldsymbol{A}_{\text{st}}$ is Hurwitz and $\boldsymbol{A}_p$ can be seen as a nonlinear perturbation on the asymptotically stable part of the χ dynamics (notice that the coefficients of $\boldsymbol{A}_p$ depend on the rigid-body states and the reference trajectory). By substituting $\gamma = \tilde{\gamma} - k_2\tilde{h} + \dot{h}_{\text{ref}}/V_{\text{ref}}$, $\alpha = \alpha^* - \tilde{\gamma} + \tilde{\alpha}$, and $Q = \tilde{Q} - k_4\tilde{\alpha} + k_2^2 V_{\text{ref}}\tilde{h} - k_2 V_{\text{ref}}\tilde{\gamma} - k_2\tilde{V}\sin\gamma - \dot{V}_{\text{ref}}\dot{h}_{\text{ref}}/V_{\text{ref}}^2 + \ddot{h}_{\text{ref}}/V_{\text{ref}}$ in Eq. (19), the χ dynamics are written as

$$\begin{aligned}\dot{\boldsymbol{\chi}} &= (\boldsymbol{A}_{\text{st}} + \boldsymbol{A}_p)\boldsymbol{\chi} + (k_2^2 V_{\text{ref}}\boldsymbol{J}_3 - k_2\boldsymbol{J}_5)\tilde{h} \\ &\quad - (\boldsymbol{J}_1 + 2\boldsymbol{J}_2\alpha^* + k_2 V_{\text{ref}}\boldsymbol{J}_3 - \boldsymbol{J}_5)\tilde{\gamma} + \boldsymbol{J}_2(\tilde{\alpha} - \tilde{\gamma})^2 \\ &\quad + (\boldsymbol{J}_1 + 2\boldsymbol{J}_2\alpha^* - k_4\boldsymbol{J}_3)\tilde{\alpha} + \boldsymbol{J}_3\tilde{Q} + (\boldsymbol{J}_4 - k_2\sin\gamma\boldsymbol{J}_3)\tilde{V} \\ &\quad + \boldsymbol{J}_0 + \boldsymbol{J}_1\alpha^* + \boldsymbol{J}_2\alpha^{*2} + (\ddot{h}_{\text{ref}}/V_{\text{ref}} - \dot{h}_{\text{ref}}\dot{V}_{\text{ref}}/V_{\text{ref}}^2)\boldsymbol{J}_3 \\ &\quad + \boldsymbol{J}_5\dot{h}_{\text{ref}}/V_{\text{ref}} \end{aligned} \tag{20}$$

A closer look at the terms on the right-hand side of Eq. (20) reveals that $(\ddot{h}_{\text{ref}}/V_{\text{ref}} - \dot{h}_{\text{ref}}\dot{V}_{\text{ref}}/V_{\text{ref}}^2)\boldsymbol{J}_3 + \boldsymbol{J}_5\dot{h}_{\text{ref}}/V_{\text{ref}}$ is a bounded perturbation vanishing at trim, whereas $\boldsymbol{J}_0 + \boldsymbol{J}_1\alpha^* + \boldsymbol{J}_2\alpha^{*2}$ is a nonvanishing term that determines the steady-state value $\boldsymbol{\chi}^*$ of $\boldsymbol{\chi}(t)$. As a result, the analysis of the stability properties of the equilibrium point $\boldsymbol{\chi} = \boldsymbol{\chi}^*$ of Eq. (20) is reduced to studying the stability properties of the origin of the nonlinear system

$$\dot{\tilde{\boldsymbol{\chi}}} = [\boldsymbol{A}_{\text{st}} + \boldsymbol{A}_p(\boldsymbol{x}, \boldsymbol{y}_{\text{ref}})]\tilde{\boldsymbol{\chi}} + B(\boldsymbol{x}, \boldsymbol{y}_{\text{ref}})\tilde{\boldsymbol{x}} \tag{21}$$

where $\tilde{\boldsymbol{\chi}} = \boldsymbol{\chi} - \boldsymbol{\chi}^*$ and

$$\boldsymbol{B}(\boldsymbol{x}, \boldsymbol{y}_{\text{ref}}) = [\,\boldsymbol{J}_4 - k_2\sin\gamma\boldsymbol{J}_3 \quad k_2^2 V_{\text{ref}}\boldsymbol{J}_3 - k_2\boldsymbol{J}_5 \quad \boldsymbol{J}_2\tilde{\gamma} - 2\boldsymbol{J}_2\tilde{\alpha} - \boldsymbol{J}_1 - 2\boldsymbol{J}_2\alpha^* - k_2 V_{\text{ref}}\boldsymbol{J}_3 + \boldsymbol{J}_5 \quad \boldsymbol{J}_2\tilde{\alpha} + \boldsymbol{J}_1 + 2\boldsymbol{J}_2\alpha^* - k_4\boldsymbol{J}_3 \quad \boldsymbol{J}_3\,]$$

System (21) is the required representation of the internal dynamics of the closed-loop system, which arises when the structural flexibilities are taken into consideration.

A. Stability Analysis of the Zero Dynamics

A necessary step toward the analysis of the interconnection of systems (13) and (21) is the investigation of the stability of its zero dynamics, that is, the system

$$\dot{\tilde{\boldsymbol{\chi}}} = [\boldsymbol{A}_{\text{st}} + \boldsymbol{A}_p(\boldsymbol{x}, \boldsymbol{y}_{\text{ref}})]\tilde{\boldsymbol{\chi}} \tag{22}$$

obtained by setting $\tilde{\boldsymbol{x}} = 0$ in Eq. (21). A Lyapunov function candidate for Eq. (22) is obtained from the Lyapunov equation for the Hurwitz matrix $\boldsymbol{A}_{\text{st}}$. Specifically, the matrices

$$\boldsymbol{A}_i = \begin{bmatrix} 0 & 1 \\ -\omega_i^2 & -2\zeta_i\omega_i \end{bmatrix}$$

$$\boldsymbol{P}_i = \begin{bmatrix} \dfrac{1 + \omega_i^2 + 4\zeta_i^2}{4\zeta_i\omega_i} & \dfrac{1}{2\omega_i^2} \\ \dfrac{1}{2\omega_i^2} & \dfrac{1 + \omega_i^2}{4\zeta_i\omega_i^3} \end{bmatrix}, \qquad i = 1, 2, 3$$

satisfy the Lyapunov equation $\boldsymbol{P}_i\boldsymbol{A}_i + \boldsymbol{A}_i^T\boldsymbol{P}_i = -\boldsymbol{I}_{2\times 2}$, and $\boldsymbol{P}_i$ is positive definite because $\zeta_i > 0$. Recalling that $\boldsymbol{A}_{\text{st}} = \text{diag}\{\boldsymbol{A}_1, \boldsymbol{A}_2, \boldsymbol{A}_3\}$, the Lyapunov function candidate for system (22) is selected as

$$W_f(\tilde{\boldsymbol{\chi}}) = \sigma_\chi\tilde{\boldsymbol{\chi}}^T\boldsymbol{P}\tilde{\boldsymbol{\chi}} \tag{23}$$

where $\boldsymbol{P} := \text{diag}\{\boldsymbol{P}_1, \boldsymbol{P}_2, \boldsymbol{P}_3\}$, and σ_χ is a positive scaling factor. By construction, the derivative of W_f along the vector field of system (22) satisfies

$$\dot{W}_f(\tilde{\boldsymbol{\chi}}) = -\sigma_\chi\tilde{\boldsymbol{\chi}}^T[\boldsymbol{I}_{6\times 6} - (\boldsymbol{P}\boldsymbol{A}_p^T + \boldsymbol{A}_p\boldsymbol{P})]\tilde{\boldsymbol{\chi}}$$

Therefore, the origin of system (22) is asymptotically stable if the perturbation $\boldsymbol{A}_p$ is small enough to satisfy $\boldsymbol{P}\boldsymbol{A}_p^T + \boldsymbol{A}_p\boldsymbol{P} < \boldsymbol{I}_{6\times 6}$. Note that the entries of $\boldsymbol{A}_p$ depend on the model parameters, $\bar{q}$, V, and V_{ref}. Thus, the aforementioned Lyapunov equation gives a method to ascertain the stability of the internal dynamics in terms of the current and desired flight conditions.

For the model under investigation, it has been verified numerically that the aforementioned stability condition on the matrix $\boldsymbol{A}_p$ holds in the feasible set $\mathcal{A}$ and for all $\boldsymbol{p} \in \mathcal{P}$. Consequently, the origin of system (22) is robustly asymptotically stable, and there exists a

constant symmetric and positive definite matrix $\bar{\boldsymbol{R}}_f$ such that, for any $\boldsymbol{x} \in \mathcal{A}$ and $\boldsymbol{p} \in \mathcal{P}$, the derivative of $W_f(\tilde{\boldsymbol{\chi}})$ along trajectories of system (21) satisfies

$$\dot{W}_f(\tilde{\boldsymbol{\chi}}) \leq -\sigma_\chi \tilde{\boldsymbol{\chi}}^T \bar{\boldsymbol{R}}_f \tilde{\boldsymbol{\chi}} + \tilde{\boldsymbol{\chi}}^T \boldsymbol{R}_{\text{fl,rb}}(\boldsymbol{x}, \boldsymbol{y}_{\text{ref}}) \tilde{\boldsymbol{x}} \tag{24}$$

where $\boldsymbol{R}_{\text{fl,rb}}(\boldsymbol{x}, \boldsymbol{y}_{\text{ref}}) := 2\sigma_\chi \boldsymbol{P}\boldsymbol{B}(\boldsymbol{x}, \boldsymbol{y}_{\text{ref}})$.

B. Stability Analysis of the Overall Closed-Loop System

The last step of the stability analysis is to consider explicitly the overall system (13–21), because the stability of the internal dynamics and the rigid-body closed-loop system alone does not guarantee the stability of the interconnection. Unsurprisingly, the analysis is carried out by using $W(\tilde{\boldsymbol{x}}, \tilde{\boldsymbol{\chi}}, \tilde{\boldsymbol{\theta}}) = W_{\text{rb}}(\tilde{\boldsymbol{x}}, \tilde{\boldsymbol{\theta}}) + W_f(\tilde{\boldsymbol{\chi}})$ as a Lyapunov function candidate.

Let $\Omega_c(W) = \{\tilde{\boldsymbol{x}}, \tilde{\boldsymbol{\chi}}, \tilde{\boldsymbol{\theta}} | W(\tilde{\boldsymbol{x}}, \tilde{\boldsymbol{\chi}}, \tilde{\boldsymbol{\theta}}) \leq c\}$ be the level set corresponding to the value $c > 0$ defined in Sec. IV, so that conditions a1–a3 continue to hold with W replacing W_{rb}, and choose $\sigma_\chi > 0$ small enough so that $\Xi_0^{\tilde{\eta}} \subset \Omega_c(W)$. As a result, condition a1 is replaced by b1) $\Xi_0^{\tilde{x}} \times \Xi_0^{\tilde{\eta}} \subset \Omega_c(W)$, for all $\boldsymbol{x} \in \mathcal{A}$, $\boldsymbol{p} \in \mathcal{P}$.

As mentioned, the particular structure of the matrices $\boldsymbol{B}_X$ and $\boldsymbol{D}_X$ employed in the transformation (17) plays an important role. Looking at the definition of the vectors $\boldsymbol{C}_i^\eta$, $i = T, M, L$, and D, in Eq. (3), it is immediately concluded that $\boldsymbol{C}_i^\eta \boldsymbol{B}_X = 0$ and $\boldsymbol{C}_i^\eta D_X = 0$. This, in turn, implies that $\boldsymbol{C}_i^\eta \boldsymbol{\eta} = \boldsymbol{C}_i^\eta \boldsymbol{\chi}$, and, because the trim value $\boldsymbol{\chi}^* = \boldsymbol{\eta}^* - \boldsymbol{B}_X \boldsymbol{G}_1^{-1}(V^*)[\alpha^* \quad 0]^T$ satisfies $\chi^*_{2i-1} = \eta_i^*$, $i = 1, 2, 3$, this also implies $\boldsymbol{C}_i^\eta \tilde{\boldsymbol{\eta}} = \boldsymbol{C}_i^\eta \tilde{\boldsymbol{\chi}}$, $i = T, M, L, D$. As a result, the derivative of W along trajectories of system (13–21) satisfies

$$\dot{W}(\tilde{\boldsymbol{x}}, \tilde{\boldsymbol{\chi}}, \tilde{\boldsymbol{\theta}}) \leq -[\tilde{\boldsymbol{\chi}}^T \quad \tilde{\boldsymbol{x}}^T] \boldsymbol{R}(\boldsymbol{x}, \boldsymbol{y}_{\text{ref}}) [\tilde{\boldsymbol{\chi}}^T \quad \tilde{\boldsymbol{x}}^T]^T \tag{25}$$

where

$$\boldsymbol{R}(\boldsymbol{x}, \boldsymbol{y}_{\text{ref}}) = \begin{bmatrix} \sigma_\chi \bar{\boldsymbol{R}}_f & -\frac{1}{2}\boldsymbol{R}_{\text{fl,rb}}(\boldsymbol{x}, \boldsymbol{y}_{\text{ref}}) - \frac{1}{2}\boldsymbol{R}_{\text{rb,fl}}(\boldsymbol{x})^T \\ -\frac{1}{2}\boldsymbol{R}_{\text{fl,rb}}(\boldsymbol{x}, \boldsymbol{y}_{\text{ref}})^T - \frac{1}{2}\boldsymbol{R}_{\text{rb,fl}}(\boldsymbol{x}) & \boldsymbol{R}_{\text{rb}}(\boldsymbol{x}) \end{bmatrix}$$

It is important to notice that the off-diagonal terms of the matrix $\boldsymbol{R}(\boldsymbol{x}, \boldsymbol{y}_{\text{ref}})$ depend on the controller gains k_2 and k_4 relative to the altitude and angle of attack loops. Consequently, the influence of these gains on the stability of the closed-loop system is fundamentally different from the case analyzed in Proposition III.1, in which the internal dynamics were ignored. The following proposition constitutes the main result of the paper:

Proposition IV.1: Consider the closed-loop system given by Eqs. (13) and (21), and the Lyapunov function candidate $W(\tilde{\boldsymbol{x}}, \tilde{\boldsymbol{\chi}}, \tilde{\boldsymbol{\theta}})$. Let the level set $\Omega_c(W)$ and the scaling factors of W be chosen to satisfy conditions b1, a2, and a3. Then, there exist constants $k_1^\star > 0$, $k_2^\star > 0$, $k_3^\star > 0$, $k_5^\star > 0$, and $0 < \underline{k}_4^\star < \bar{k}_4^\star$ such that, for any $k_1 > k_1^\star$, $0 < k_2 < k_2^\star$, $k_3 > k_3^\star$, $\underline{k}_4^\star < k_4 < \bar{k}_4^\star$, and $k_5 > k_5^\star$, the trajectories of the closed-loop system originating within $\Omega_c(W)$ are bounded and satisfy $\lim_{t\to\infty} \tilde{\boldsymbol{x}}(t) = 0$, $\lim_{t\to\infty} \tilde{\boldsymbol{\eta}}(t) = 0$.

Proof. To proceed with the analysis, we define the upper bounds on the off-diagonal terms of $\boldsymbol{R}$ as follows:

$$\begin{aligned}
R_V(k_2) &:= \max_{\boldsymbol{x}\in\mathcal{A},\boldsymbol{p}\in\mathcal{P}} \{\sigma_\chi \|\boldsymbol{P}\| \|\boldsymbol{J}_4 - k_2 \sin\gamma \boldsymbol{J}_3\| \\
&\quad + (\bar{q}S\sigma_V/2)\|\boldsymbol{C}_T^\eta \cos\alpha - \boldsymbol{C}_D^\eta\|\} \\
R_h(k_2) &:= \sigma_\chi k_2 \max_{\boldsymbol{x}\in\mathcal{A},\boldsymbol{p}\in\mathcal{P}} \{\|\boldsymbol{P}\boldsymbol{J}_5\| + V_{\text{ref}} \|\boldsymbol{P}\boldsymbol{J}_3\| k_2\} \\
R_\gamma(k_2) &:= \max_{\boldsymbol{x}\in\mathcal{A},\boldsymbol{p}\in\mathcal{P}} \{\sigma_\chi \|\boldsymbol{P}\| \|\boldsymbol{J}_1 + (2\tilde{\alpha} + 2\alpha^* - \tilde{\gamma})\boldsymbol{J}_2 \\
&\quad + k_2 V_{\text{ref}} \boldsymbol{J}_3 - \boldsymbol{J}_5\| + \bar{q}S\|\boldsymbol{C}_T^\eta \sin\alpha^* + \boldsymbol{C}_L^\eta\|/(2V)\} \\
R_\alpha(k_4) &:= \max_{\boldsymbol{x}\in\mathcal{A},\boldsymbol{p}\in\mathcal{P}} \{\sigma_\chi \|\boldsymbol{P}\| \|\boldsymbol{J}_1 + (\tilde{\alpha} + 2\alpha^*)\boldsymbol{J}_2\| + \sigma_\chi \|\boldsymbol{P}\boldsymbol{J}_3\| k_4\} \\
R_Q &:= \max_{\boldsymbol{x}\in\mathcal{A},\boldsymbol{p}\in\mathcal{P}} \{\sigma_\chi \|\boldsymbol{P}\boldsymbol{J}_3\| + \bar{q}S\sigma_Q \|z_T \boldsymbol{C}_T^\eta + \bar{c}\boldsymbol{C}_M^\eta\|/(2I_{yy})\}
\end{aligned}$$

and let for notational convenience $V_{\min} := \min_{\mathcal{A}} V = \min_{\mathcal{A}} V_{\text{ref}}$, and

$$R_h(k_2) := \sigma_\chi k_2 (R_{\gamma_0} + R_{\gamma_1} k_2), \qquad R_\alpha(k_4) := (\sigma_\chi R_{\alpha_0} + \sigma_\chi R_{\alpha_1} k_4)$$

Rearranging the elements of the vector $\tilde{\boldsymbol{x}}$ and considering the norms term by term, inequality (25) can be further bounded as

$$\dot{W}(\tilde{\boldsymbol{x}}, \tilde{\boldsymbol{\chi}}, \tilde{\boldsymbol{\theta}}) \leq -[\|\tilde{\boldsymbol{\chi}}\| |\tilde{h}| |\tilde{\alpha}| |\tilde{\gamma}| |\tilde{Q}| |\tilde{V}|] \bar{\boldsymbol{R}} [\|\tilde{\boldsymbol{\chi}}\| |\tilde{h}| |\tilde{\alpha}| |\tilde{\gamma}| |\tilde{Q}| |\tilde{V}|]^T$$

where

$$\bar{\boldsymbol{R}} = \begin{bmatrix} \sigma_\chi \lambda_f & -R_h(k_2) & -R_\alpha(k_4) & -R_\gamma(k_2) & -R_Q & -R_V(k_2) \\ -R_h(k_2) & k_2\sigma_h V_{\min} & 0 & -R_{13}^{\text{rb}} & 0 & -R_{15}^{\text{rb}} \\ -R_\alpha(k_4) & 0 & \sigma_\alpha k_4 & -R_{23}^{\text{rb}} & -R_{24}^{\text{rb}}(k_4) & 0 \\ -R_\gamma(k_2) & -R_{13}^{\text{rb}} & -R_{23}^{\text{rb}} & (k_m + k_c k_3) V_{\min} & 0 & 0 \\ -R_Q & 0 & -R_{24}^{\text{rb}}(k_4) & 0 & \sigma_Q(k_5 - k_4) & 0 \\ -R_V(k_2) & -R_{15}^{\text{rb}} & 0 & 0 & 0 & k_1\sigma_V \end{bmatrix}$$

$$R_{13}^{\text{rb}} = \frac{\sigma_h \max_{\mathcal{A}} V_{\text{ref}}}{2} \qquad R_{15}^{\text{rb}} = \frac{\sigma_h \max_{\mathcal{A}} |\gamma|}{2} \qquad R_{23}^{\text{rb}} = \frac{k_M \max_{\mathcal{A}} V}{2} \qquad R_{24}^{\text{rb}}(k_4) = \frac{|\sigma_\alpha - \sigma_Q k_4^2|}{2}$$

and $\lambda_f > 0$ denotes the smallest eigenvalue of $\bar{\boldsymbol{R}}_f$. As before, let Δ_i denote the determinant associated with the ith order upper-left submatrix of $\bar{R}$. Clearly, $\Delta_1 = \sigma_\chi \lambda_f > 0$. Because

$$\begin{aligned}
\Delta_2 &= \sigma_\chi \sigma_h \lambda_f k_2 V_{\min} - R_h^2(k_2) \\
&= \sigma_\chi \sigma_h \lambda_f k_2 V_{\min} - \sigma_\chi^2 k_2^2 (R_{\gamma_0} + R_{\gamma_1} k_2)^2
\end{aligned}$$

it follows that for any λ_f, σ_h, $\sigma_\chi > 0$ there exists $k_2^\star > 0$ such that $\sigma_\chi k_2^\star (R_{\gamma_0} + R_{\gamma_1} k_2^\star)^2 < \sigma_h \lambda_f V_{\min}$. Therefore, Δ_2 is positive for any $0 < k_2 < k_2^\star$. On the other hand, the determinant Δ_3, given by

$$\begin{aligned}
\Delta_3 &= \Delta_2 \sigma_\alpha k_4 - k_2 \sigma_h V_{\min} R_\alpha^2(k_4) \\
&= [\sigma_\chi \sigma_h \lambda_f k_2 V_{\min} - \sigma_\chi^2 k_2^2 (R_{\gamma_0} + R_{\gamma_1} k_2)^2] \sigma_\alpha k_4 \\
&\quad - k_2 \sigma_h V_{\min} \sigma_\chi^2 (R_{\alpha_0} + R_{\alpha_1} k_4)^2
\end{aligned}$$

is strictly positive if and only if the quadratic function of k_4 defined as

$$\begin{aligned}
f(k_4) &:= \sigma_h \sigma_\chi V_{\min} R_{\alpha_1}^2 k_4^2 \\
&\quad + [2\sigma_h \sigma_\chi V_{\min} R_{\alpha_0} R_{\alpha_1} + \sigma_\chi \sigma_\alpha k_2 (R_{\gamma_0} + R_{\gamma_1} k_2)^2 \\
&\quad - \sigma_h \sigma_\alpha \lambda_f V_{\min}] k_4 + \sigma_h \sigma_\chi V_{\min} R_{\alpha_0}^2
\end{aligned}$$

is strictly negative. This condition, unlike the ones found so far, cannot be satisfied simply by increasing or decreasing k_4. In particular, it is necessary to analyze the function $f(k_4)$ to verify that

Table 2 Initial and desired final conditions for the regulated output and dynamic pressure

	Case study 1		Case study 2	
Variable	Initial condition (trim)	Final trim	Initial condition	Final trim
V	7850 ft/s	10640 ft/s	7850 ft/s	10500 ft/s
h	86,000 ft	99,000 ft	8,6000 ft	111,000 ft
α	1.36 deg	1.71 deg	2 deg	1.5 deg
$\bar{q}$	1982 psf	1982 psf	1982 psf	1153 psf

an interval $(\underline{k}_4^\star, \bar{k}_4^\star)$ where $f(k_4)$ is negative exists and, consequently, Δ_3 can be made positive. Because the leading coefficient of k_4 is positive, $f(k_4)$ is a concave upward parabola whose intersection with the vertical axis is $\sigma_h \sigma_\chi R_{\alpha_0}^2 > 0$. As a result, the required interval $(\underline{k}_4^\star, \bar{k}_4^\star)$ exists if and only if the following two conditions are satisfied:

$$2\sigma_h \sigma_\chi V_{\min} R_{\alpha_0} R_{\alpha_1} + \sigma_\chi \sigma_\alpha k_2 (R_{\gamma_0} + R_{\gamma_1} k_2)^2 - \sigma_h \sigma_\alpha \lambda_f V_{\min} < 0 \tag{26}$$

$$[2\sigma_h \sigma_\chi V_{\min} R_{\alpha_0} R_{\alpha_1} + \sigma_\chi \sigma_\alpha k_2 (R_{\gamma_0} + R_{\gamma_1} k_2)^2 - \sigma_h \sigma_\alpha \lambda_f V_{\min}]^2 - 4\sigma_h^2 \sigma_\chi^2 R_{\alpha_1}^2 R_{\alpha_0}^2 V_{\min}^2 > 0 \tag{27}$$

It is easy to see that, given any fixed positive value of σ_h, σ_α, λ_f, and k_2, there exists $\sigma_\chi^\star > 0$ such that conditions (26) and (27) are met for any $0 < \sigma_\chi < \sigma_\chi^\star$. This implies that there exists an interval for values of k_4, which render Δ_3 strictly positive only if a small enough σ_χ is chosen. The crucial thing to notice is that the original value of the scaling factor σ_χ can always be lowered to be made smaller than $\sigma_\chi^\star$ without shrinking the domain of attraction, that is, without affecting the property b1; thus, the interval $(\underline{k}_4^\star, \bar{k}_4^\star)$ is guaranteed to exist. Finally, notice that the determinants $(\Delta_1, \Delta_2, \Delta_3)$ do not depend on k_3, $(\Delta_1, \Delta_2, \Delta_3, \Delta_4)$ do not depend on k_5, and $(\Delta_1, \Delta_2, \Delta_3, \Delta_4, \Delta_5)$ do not depend on k_1. Consequently, for any fixed k_2, $k_4 > 0$ there exist $k_3^\star > 0$, $k_5^\star > 0$ and $k_1^\star > 0$ such that, for any $k_3 > k_3^\star$, $k_5 > k_5^\star$ and $k_1 > k_1^\star$, Δ_4, Δ_5, and Δ_6 are strictly positive. By Sylvester's criterion, it follows that matrix $\bar{\boldsymbol{R}}$ can be made positive definite by choice of the controller gains. Arguments similar to those invoked in the proof of Proposition III.1 imply that all trajectories of the closed-loop system are bounded, and that the error trajectories $\tilde{\boldsymbol{x}}(t)$, $\tilde{\boldsymbol{\chi}}(t)$ are regulated to zero asymptotically. By virtue of Eq. (17) and the fact that $\boldsymbol{\chi}^* = \boldsymbol{\eta}^* - \boldsymbol{B}_X \boldsymbol{G}_1^{-1}(V^*)[\alpha^* \quad 0]^T$, this also implies that $\tilde{\boldsymbol{\eta}}(t)$ converges to zero asymptotically. □

The existence of a finite interval for the stabilizing values of k_4 (i.e., conditional stability) and the finite stability margin for k_2 are both consequences of the peaking phenomenon [34] exhibited by the internal dynamics, which is due to the simultaneous appearance of α and Q in Eq. (19). Thus, the overall closed-loop system can not be stabilized by purely low-gain or high-gain feedback [35]. Had the peaking phenomenon not occurred, the term R_{α_0} would have been zero; therefore, Δ_3 could have been rendered positive simply by lowering the value of the gain k_4. The difference with the case in which only the rigid-body dynamics are considered in the closed-loop system is very significant, especially regarding the role of k_2. Because a nonzero value of the gain k_3 is required for stability, it is seen that the canard input plays a fundamental role for robust stabilization in the presence of structural flexibilities.

V. Simulations

The controller derived in the previous section has been tested in simulation using the full SM implemented in SIMULINK®. Two representative case studies will be presented here, corresponding, respectively, to a climbing maneuver at constant dynamic pressure and a climbing maneuver with longitudinal acceleration using separate reference commands for altitude and velocity. The initial and final trim conditions for each case study are reported in Table 2. In both cases, the reference commands have been generated by filtering step reference commands with a second-order prefilter with a natural frequency of $\omega_f = 0.03$ rad/s and a damping factor of $\zeta_f = 0.95$. In this study, the constraints are dealt with indirectly by tuning the controller gains, including the parameters of the prefilter of the reference model. The controller gains used in all simulations are shown in Table 3. To take into further account the parameter uncertainty of the CDM, the initial condition of the controller parameter vector $\hat{\boldsymbol{\theta}}$ has been selected randomly within a 40% variation of the nominal value of the parameter vector $\boldsymbol{\theta}$.

Table 3 Controller gains

Gain	Value	Gain matrix	Value
k_1	200	Γ_1	$0.1 \times \boldsymbol{I}_{16\times16}$
k_2	1×10^{-4}	Γ_2	$0.1 \times \boldsymbol{I}_{5\times5}$
k_3	10	Γ_3	$0.1 \times \boldsymbol{I}_{13\times13}$
k_4	50		
k_5	60		

In the first simulation study, the vehicle is initially at trim. The reference $h_{\text{ref}}(t)$ is generated to let the vehicle climb 13,000 ft in about 350 s, whereas the velocity reference is computed according to the relation $V_{\text{ref}}(t) = [2\bar{q}\exp((h_{\text{ref}}(t) - h_0)/h_s)/\rho_0]^{1/2}$ to maintain constant dynamic pressure at $\bar{q} = 1982$ psf throughout the maneuver. The results of the simulation confirm that the controller provides stable tracking of the reference trajectories and convergence to the desired trim condition. More specifically, the tracking performance for the velocity and altitude is shown in Figs. 5a and 5b, in which it is seen that the error remains remarkably small during the entire maneuver and vanishes asymptotically. Figure 5c shows the tracking performance of the flight-path angle command, whereas the behavior of the angle of attack is given in the top plot of Fig. 5d. It can be noted that the response of the flight-path angle exhibits the typical undershoot of the output of a nonminimum phase system. As a representative of the state variables of the adaptive controller, the bottom plot shows the time history of the crucial parameter estimate $\hat{\boldsymbol{\theta}}_{2,1}(t)$, corresponding to the coefficient $\boldsymbol{\theta}_{2,1} = C_L^{\delta_e}/C_L^{\delta_c}$, which provides cancellation of the elevator-to-lift coupling. The flexible modes $\boldsymbol{\eta}(t)$, shown in Fig. 6a, remain damped throughout the maneuver. Finally, Fig. 6b shows that the control inputs range within their bounds.

The second case study considers a more aggressive maneuver, in which the altitude and velocity reference trajectories are defined independently. In particular, $h_{\text{ref}}(t)$ is generated to let the vehicle climb 25,000 ft in about 250 s, corresponding to a climb rate approximately 3 times faster than the previous case. At the same time, $V_{\text{ref}}(t)$ provides a longitudinal acceleration of about 10 ft/s^2, which corresponds the dynamic pressure decreasing from $\bar{q} = 1982$ psf at $t = 0$ to $\bar{q} = 1153$ psf at $t = 300$. To make the test more demanding, the initial condition is selected at an off-trim condition, obtained by changing the initial value of the angle of attack to $\alpha(0) = 2$ deg while keeping the remaining values of $\boldsymbol{x}(0)$ and $\boldsymbol{u}(0)$ unchanged from the previous case study. The desired steady-state value for the angle of attack has also been decreased to $\alpha^* = 1.5$ deg. The trim condition reached at the end of the maneuver is shown in the last column of Table 2. The results of the simulation are shown in Fig. 7. The closed-loop behavior remains excellent, although the tracking error exhibits a slightly worse transient behavior. This is to be expected, due to the more demanding control objective and the fact that the initial condition is not at an equilibrium. In particular, note that the flexible states remain well

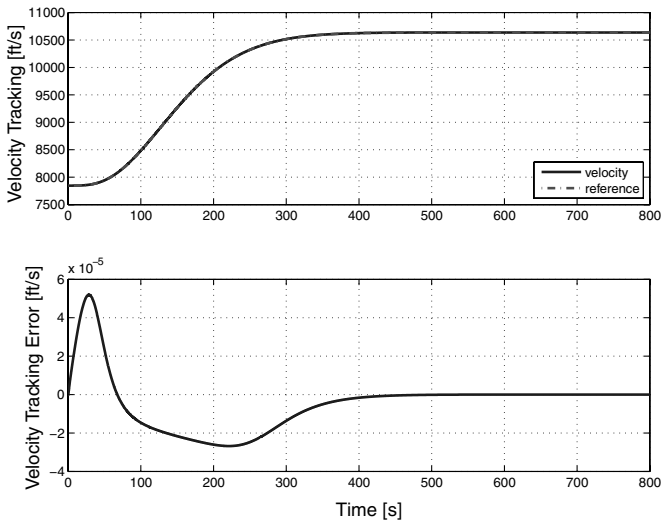

a) $V(t)$ and $V_{ref}(t)$ (top), and $\tilde{V}(t)$ (bottom)

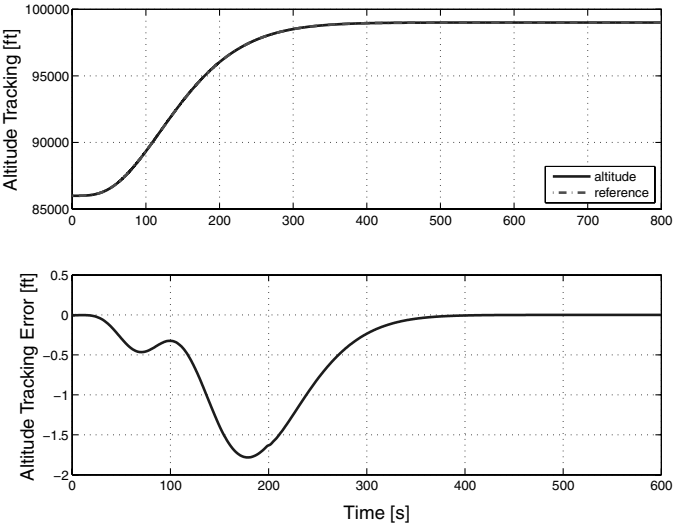

b) $h(t)$ and $h_{ref}(t)$ (top), and $\tilde{h}(t)$ (bottom)

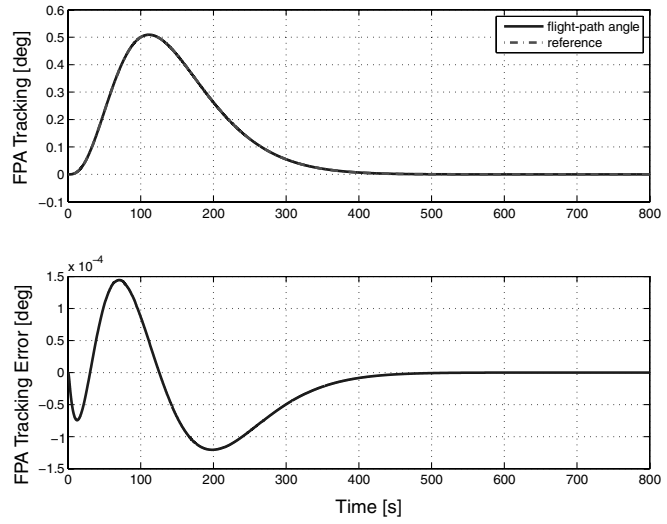

c) $\gamma(t)$ and $\gamma_{cmd}(t)$ (top), and $\tilde{\gamma}(t)$ (bottom)

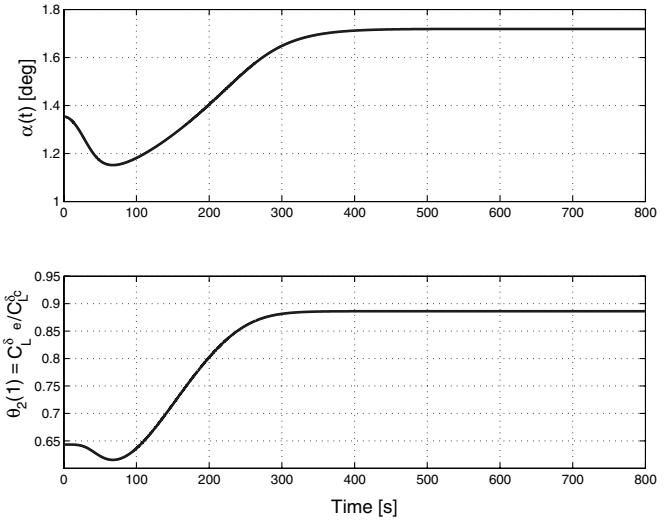

d) $\alpha(t)$ (top) and $\hat{\theta}_{2,1}(t)$ (bottom)

Fig. 5 Adaptive controller; climb at constant dynamic pressure $\bar{q} = 1982$ psf for case study 1: a) velocity, b) altitude, c) flight-path angle tracking performance, and d) angle of attack and parameter estimate $\hat{\theta}_{1,2}$.

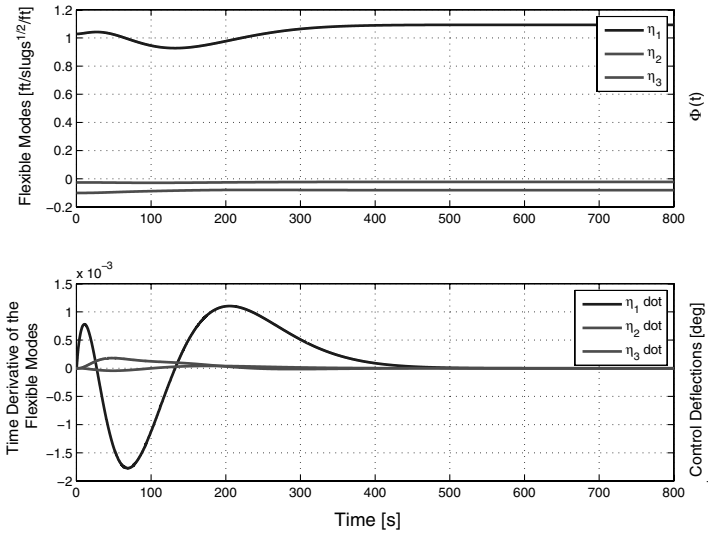

a) $\eta(t)$ (top) and $\dot{\eta}(t)$ (bottom)

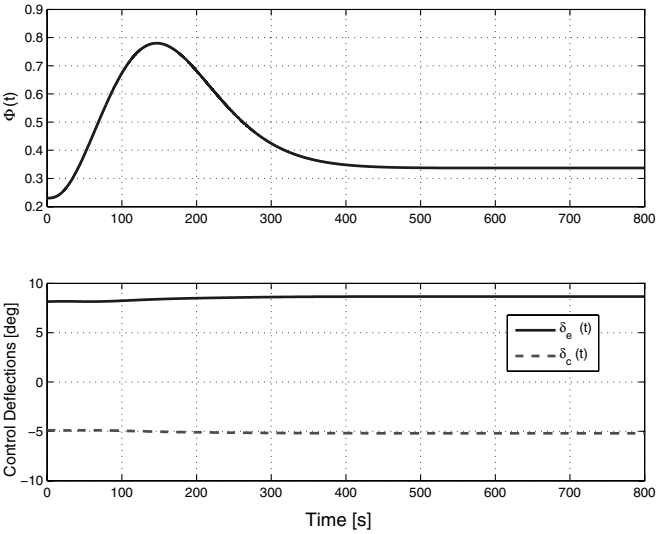

b) $\Phi(t)$ (top) and $\delta_c(t), \delta_e(t)$ (bottom)

Fig. 6 Adaptive controller; climb at constant dynamic pressure $\bar{q} = 1982$ psf for case study 1: a) flexible modes, and b) control inputs.

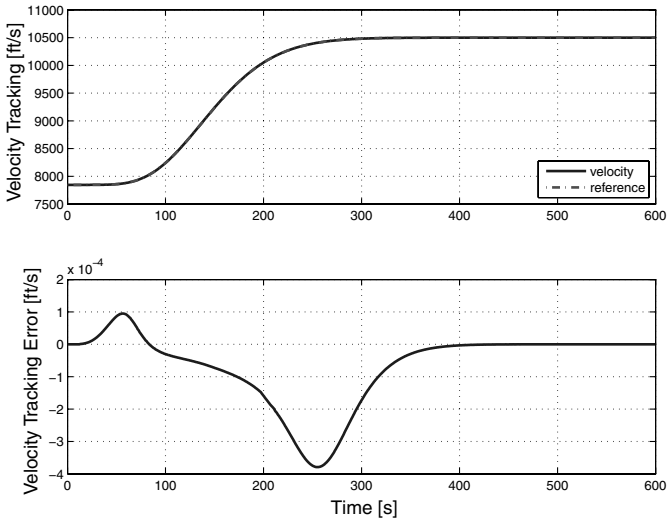

a) $V(t)$ and $V_{\mathbf{ref}}(t)$ (top), and $\tilde{V}(t)$ (bottom)

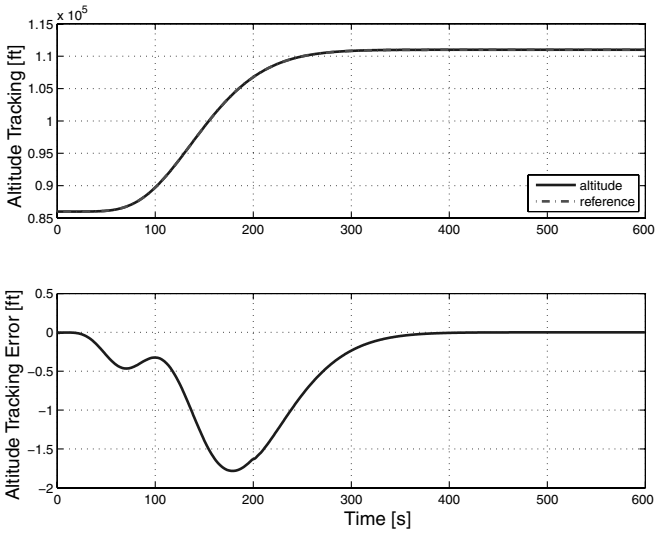

b) $h(t)$ and $h_{\mathbf{ref}}(t)$ (top), and $\tilde{h}(t)$ (bottom)

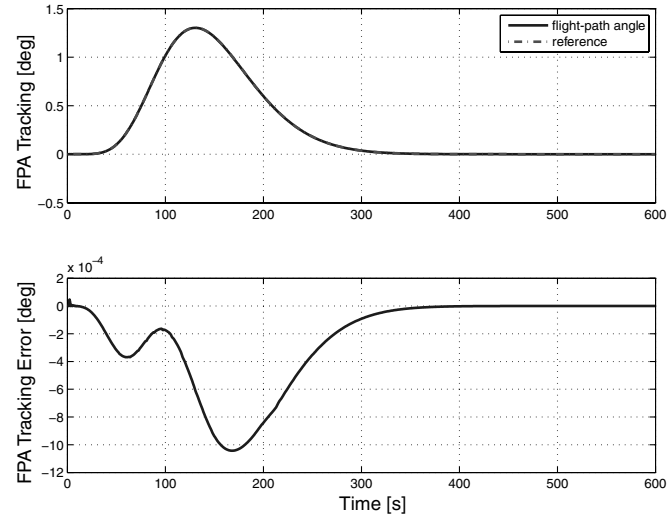

c) $\gamma(t)$ and $\gamma_{\mathbf{cmd}}(t)$ (top), and $\tilde{\gamma}$ (t) (bottom)

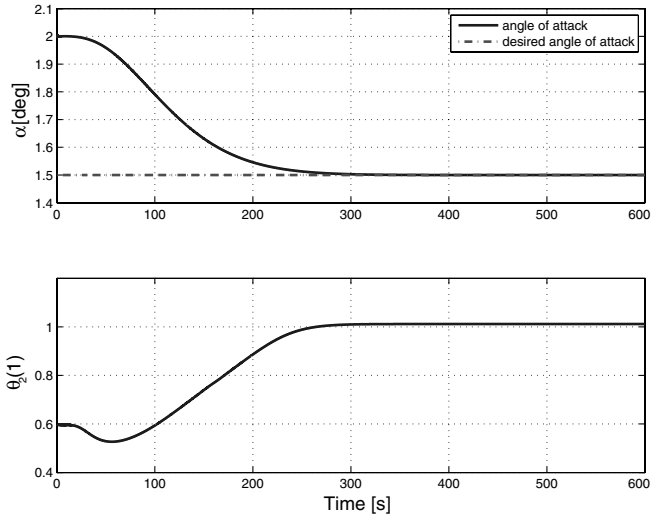

d) $\alpha(t)$ (top) and $\hat{\theta}_{\mathbf{2,1}}$ (t) (bottom)

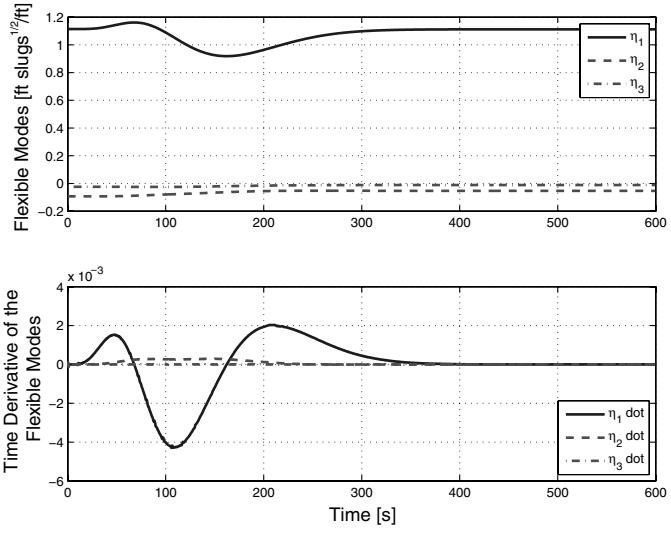

e) $\eta(t)$ (top) and $\dot{\eta}(t)$ (bottom)

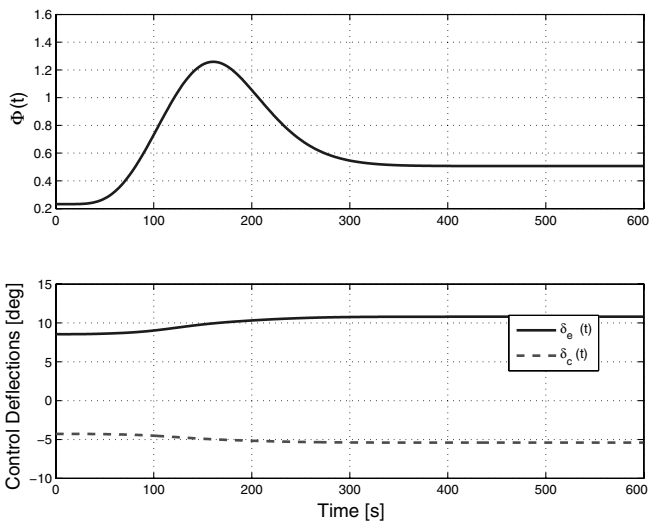

f) $\Phi(t)$ (top) and $\delta_c(t)$, $\delta_e(t)$ (bottom)

Fig. 7 Adaptive controller; climb and acceleration at varying dynamic pressure for case study 2: a) velocity, b) altitude, c) flight-path angle tracking performance, d) angle of attack and parameter estimate $\hat{\theta}_{1,2}$, e) flexible modes, and f) control inputs.

behaved despite a larger excitation (see Fig. 7e). Finally, the performance of the adaptive controller in these two case studies has been compared with the results obtained using the approximate feedback linearization controller developed in Parker et al [27]. For this scheme, the control law is composed of a fixed-structure dynamic inversion inner loop and an outer-loop linear quadratic regulator controller with integral error augmentation. The canard is ganged to the elevator to provide cancellation of the elevator-to-lift

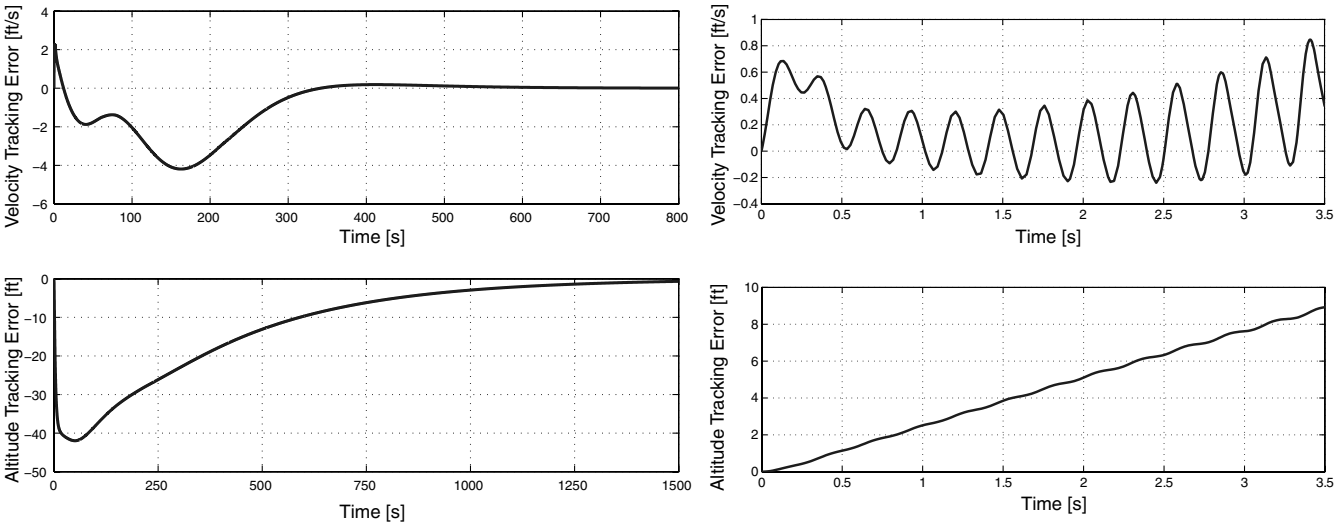

a) $\tilde{V}(t)$ (top) and $\tilde{h}(t)$ (bottom), case study 1 **b) $\tilde{V}(t)$ (top) and $\tilde{h}(t)$ (bottom), case study 2**

Fig. 8 Approximate feedback linearization controller [27]; tracking error $\tilde{V}(t)$ and $\tilde{h}(t)$: a) case study 1, and b) case study 2.

coupling, computed on the basis of the nominal values of the parameters of the CDM. For case study 1, simulation results obtained with the approximate dynamic inversion controller are comparable to those obtained with the adaptive controller, although the former exhibits a larger error during transient, and the altitude error takes substantially longer to converge (see Fig. 8a). On the other hand, for the more-demanding control objective in case study 2, the fixed linearization scheme is not capable of providing enough robustness to maintain stable tracking of the reference, as is visible in Fig. 8b, showing the onset of instability. The simulation stops at about $t = 3.5$ s due to the fact that the engine reaches a condition that no longer sustains scramjet propulsion. The reason for closed-loop instability can be attributed to the effect of model uncertainty leading to imperfect compensation of the nonminimum phase behavior and to the resulting interaction of the pitch dynamics with the structural dynamics. The domain of attraction provided by the fixed controller is reduced due to residual undesired coupling. This phenomenon was also observed in [27], in which a fine tuning of the gain of the canard input for a given reference trajectory was required to obtain a stable behavior. The adaptive controller presented in this work avoids the necessity of such gain scheduling, as it compensates automatically for the model mismatch.

VI. Conclusions

Robust stability against parameter and dynamic uncertainty is a fundamental issue when adopting a reduced-order or reduced-complexity model for control systems design. For the hypersonic vehicle model considered in this study, this aspect has been fully addressed by developing an analytical control-oriented model that can be used for both nonlinear control design and quantitative stability analysis. For controller design, we have followed an approach that combines robust adaptive dynamic inversion with back-stepping arguments to obtain a control architecture that uses the natural decomposition of the longitudinal vehicle dynamics into velocity, altitude/flight-path angle, and angle-of-attack/pitch rate subsystems. The issue of model mismatch when performing dynamic inversion is satisfactorily addressed as a result of stable adaptation in the controller parameters. Crucial to the applicability of the methodology is the explicit derivation of the internal dynamics of the model due to the presence of the flexible dynamics in the control-design model and its incorporation into a comprehensive Lyapunov-based stability analysis. As in our previous work, and in much of the literature, the controller developed in this paper makes use of feedback from the rigid-body states only and does not resort to active damping of the structure from either direct or estimated elastic mode amplitudes. Consequently, it is of paramount importance to assess the impact of the structural dynamics on the closed-loop system and to determine bounds for the controller gains that guarantee a stable operation. The approach pursued in this paper makes it possible to obtain these gain margins directly from the Lyapunov analysis. This feature sets this study apart from similar works on nonlinear control design for this class of vehicles, for which the effect of the structural dynamics on the robustness of the stability of the closed-loop system is only assessed in simulation; therefore, the evaluation of the gain margins is left to a trial-and-error procedure. It is noteworthy that the results of the stability analysis differ greatly if the closed-loop system includes only the rigid-body dynamics, as in this case infinite gain margins are predicted, whereas conditional stability with respect to the altitude and pitch rate loop gains is observed with structural flexibilities in place. The occurrence of conditional stability has been verified in simulation, as instability arises if the pitch rate gain is increased beyond its computed upper bound.

Appendix: Flexible Dynamics Vectors

The expression of the vectors in Eq. (19) are given by

$$\boldsymbol{J}_0 = \begin{bmatrix} 0 \\ \bar{q}S[N_1^0 - C_B C_D^0 N_1^{L\delta}] - \bar{q}SC_A[N_1^{L\delta} C_M^0 - (V_{\text{ref}}/V)N_1^{M\delta} C_L^0] - C_A mg(V_{\text{ref}}/V)N_1^{M\delta}\cos\gamma - mC_B N_1^{L\delta}\dot{V}_{\text{ref}} \\ 0 \\ \bar{q}S[N_2^0 - C_B C_D^0 N_2^{L\delta}] - \bar{q}SC_A[N_2^{L\delta} C_M^0 - (V_{\text{ref}}/V)N_2^{M\delta} C_L^0] - C_A mg(V_{\text{ref}}/V)N_2^{M\delta}\cos\gamma - mC_B N_2^{L\delta}\dot{V}_{\text{ref}} \\ 0 \\ \bar{q}S[N_3^0 - C_B C_D^0 N_3^{L\delta}] - \bar{q}SC_A[N_3^{L\delta} C_M^0 - (V_{\text{ref}}/V)N_3^{M\delta} C_L^0] - C_A mg(V_{\text{ref}}/V)N_3^{M\delta}\cos\gamma - mC_B N_3^{L\delta}\dot{V}_{\text{ref}} \end{bmatrix}$$

$$\boldsymbol{J}_1 = \begin{bmatrix} C_A m V_{\text{ref}} N_1^{M\delta} \\ \bar{q}S[N_1^{\alpha} - C_B C_D^{\alpha} N_1^{L\delta}] - \bar{q}SC_A[N_1^{L\delta} C_M^{\alpha} - (V_{\text{ref}}/V) N_1^{M\delta} K_{\alpha_2}] - C_A m N_1^{M\delta}[2\omega_1 \zeta_1 V_{\text{ref}} + \dot{V}_{\text{ref}}] \\ C_A m V_{\text{ref}} N_2^{M\delta} \\ \bar{q}S[N_2^{\alpha} - C_B C_D^{\alpha} N_2^{L\delta}] - \bar{q}SC_A[N_2^{L\delta} C_M^{\alpha} - (V_{\text{ref}}/V) N_2^{M\delta} K_{\alpha_2}] - C_A m N_2^{M\delta}[2\omega_2 \zeta_2 V_{\text{ref}} + \dot{V}_{\text{ref}}] \\ C_A m V_{\text{ref}} N_3^{M\delta} \\ \bar{q}S[N_3^{\alpha} - C_B C_D^{\alpha} N_3^{L\delta}] - \bar{q}SC_A[N_3^{L\delta} C_M^{\alpha} - (V_{\text{ref}}/V) N_3^{M\delta} K_{\alpha_2}] - C_A m N_3^{M\delta}[2\omega_3 \zeta_3 V_{\text{ref}} + \dot{V}_{\text{ref}}] \end{bmatrix}$$

$$\boldsymbol{J}_2 = \bar{q}S \begin{bmatrix} 0 \\ N_1^{\alpha^2} - C_B C_D^{\alpha^2} N_1^{L\delta} - C_A N_1^{L\delta} C_M^{\alpha^2} \\ 0 \\ N_2^{\alpha^2} - C_B C_D^{\alpha^2} N_2^{L\delta} - C_A N_2^{L\delta} C_M^{\alpha^2} \\ 0 \\ N_3^{\alpha^2} - C_B C_D^{\alpha^2} N_3^{L\delta} - C_A N_3^{L\delta} C_M^{\alpha^2} \end{bmatrix}$$

$$\boldsymbol{J}_3 = C_A \begin{bmatrix} (I_{yy}/\bar{c}) N_1^{L\delta} \\ -m V_{\text{ref}} N_1^{M\delta} - 2\omega_1 \zeta_1 (I_{yy}/\bar{c}) N_1^{L\delta} \\ (I_{yy}/\bar{c}) N_2^{L\delta} \\ -m V_{\text{ref}} N_2^{M\delta} - 2\omega_2 \zeta_2 (I_{yy}/\bar{c}) N_2^{L\delta} \\ (I_{yy}/\bar{c}) N_3^{L\delta} \\ -m V_{\text{ref}} N_3^{M\delta} - 2\omega_3 \zeta_3 (I_{yy}/\bar{c}) N_3^{L\delta} \end{bmatrix}$$

$$\boldsymbol{J}_4 = mC_B \begin{bmatrix} -N_1^{L\delta} \\ 2\omega_1 \zeta_1 N_1^{L\delta} \\ -N_2^{L\delta} \\ 2\omega_2 \zeta_2 N_2^{L\delta} \\ -N_3^{L\delta} \\ 2\omega_3 \zeta_3 N_3^{L\delta} \end{bmatrix} \qquad \boldsymbol{J}_5 = -mgC_B \begin{bmatrix} 0 \\ N_1^{L\delta} \\ 0 \\ N_2^{L\delta} \\ 0 \\ N_3^{L\delta} \end{bmatrix}$$

Acknowledgments

This work has been supported in part by the U.S. Air Force Research Laboratories and the U.S. Air Force Office of Scientific Research through the Collaborative Center of Control Science at Ohio State University (contract F33615-01-2-3154) and a subcontract from the Michigan/U.S. Air Force Research Laboratory Collaborative Center in Control Science. The authors would also like to thank David Sigthorsson for developing the curve-fitted model.

References

[1] Chavez, F. R., and Schmidt, D. K., "Analytical Aeropropulsive/Aeroelastic Hypersonic-Vehicle Model with Dynamic Analysis," *Journal of Guidance, Control, and Dynamics*, Vol. 17, No. 6, 1994, pp. 1308–1319. doi:10.2514/3.21349

[2] Chavez, F. R., and Schmidt, D. K., "Uncertainty Modeling for Multivariable-Control Robustness Analysis of Elastic High-Speed Vehicles," *Journal of Guidance, Control, and Dynamics*, Vol. 22, No. 1, 1999, pp. 87–95. doi:10.2514/2.4354

[3] Bolender, M. A., and Doman, D. B., "A Nonlinear Longitudinal Dynamical Model of an Air-breathing Hypersonic Vehicle," *Journal of Spacecraft and Rockets*, Vol. 44, No. 2, 2007, pp. 374–387. doi:10.2514/1.23370

[4] McNamara, J., and Friedmann, P., "Aeroelastic and Aerothermoelastic Analysis of Hypersonic Vehicles: Current Status and Future Trends," AIAA Paper 2007-2013, 2007.

[5] Schmidt, D. K., "Dynamics and Control of Hypersonic Aeropropulsive/Aeroelastic Vehicles," AIAA Paper 1992-4326, 1992.

[6] Schmidt, D. K., "Optimum Mission Performance and Multivariable Flight Guidance for Airbreathing Launch Vehicles," *Journal of Guidance, Control, and Dynamics*, Vol. 20, No. 6, 1997, pp. 1157–1164. doi:10.2514/2.4171

[7] Heeg, J., Gilbert, M. G., and Pototzky, A. S., "Active Control of Aerothermoelastic Effects for a Conceptual Hypersonic Aircraft," *Journal of Aircraft*, Vol. 30, No. 4, 1993, pp. 453–458. doi:10.2514/3.56890

[8] Buschek, H., and Calise, A. J., "Uncertainty Modeling and Fixed-Order Controller Design for a Hypersonic Vehicle Model," *Journal of Guidance, Control, and Dynamics*, Vol. 20, No. 1, 1997, pp. 42–8. doi:10.2514/2.4016

[9] Lind, R., Buffington, J., and Sparks, A., "Multi-Loop Aeroservoelastic Control of a Hypersonic Vehicle," AIAA Paper 1999-4123, 1999.

[10] Lind, R., "Linear Parameter-Varying Modeling and Control of Structural Dynamics with Aerothermoelastic Effects," *Journal of Guidance, Control, and Dynamics*, Vol. 25, No. 4, 2002, pp. 733–739. doi:10.2514/2.4940

[11] Mooij, E., "Numerical Investigation of Model Reference Adaptive Control for Hypersonic Aircraft," *Journal of Guidance, Control, and Dynamics*, Vol. 24, No. 2, 2001, pp. 315–323. doi:10.2514/2.4714

[12] Groves, K. P., Sigthorsson, D. O., Serrani, A., Yurkovich, S., Bolender, M. A., and Doman, D. B., "Reference Command Tracking for a Linearized Model of an Air-Breathing Hypersonic Vehicle," AIAA Paper 2005-6144, 2005.

[13] Groves, K. P., Serrani, A., Yurkovich, S., Bolender, M. A., and Doman, D. B., "Anti-Windup Control for an Air-Breathing Hypersonic Vehicle Model," AIAA Paper 2006-6557, 2006.

[14] Sigthorsson, D. O., Serrani, A., Yurkovich, S., Bolender, M. A., and Doman, D. B., "Tracking Control for an Overactuated Hypersonic Air-Breathing Vehicle with Steady State Constraints," AIAA Paper 2006-6558, 2006.

[15] Sigthorsson, D., Jankovsky, P., Serrani, A., Yurkovich, S., Bolender, M., and Doman, D., "Robust Linear Output Feedback Control of an Airbreathing Hypersonic Vehicle," *Journal of Guidance, Control, and Dynamics*, Vol. 31, No. 4, 2008, pp. 1052–1066. doi:10.2514/1.32300

[16] Kuipers, M., Mirmirani, M., Ioannou, P., and Huo, Y., "Adaptive Control of an Aeroelastic Airbreathing Hypersonic Cruise Vehicle," AIAA Paper 2007-6326, 2007.

[17] Mirmirani, M., Wu, C., Clark, A., Choi, S., and Colgren, R., "Modeling for Control of a Generic Airbreathing Hypersonic Vehicle," AIAA Paper 2005-6256, 2005.

[18] Cockrell, C., Jr., Engelund, W., Bittner, R., Jentink, T., Dilley, A., and Frendi, A., "Integrated Aeropropulsive Computational Fluid Dynamics Methodology for the Hyper-X Flight Experiment," *Journal of Spacecraft and Rockets*, Vol. 38, No. 6, 2001, pp. 836–843. doi:10.2514/2.3773

[19] Engelund, W., Holland, S., Cockrell Jr, C., and Bittner, R., "Aerodynamic Database Development for the Hyper-X Airframe-Integrated Scramjet Propulsion Experiments," *Journal of Spacecraft and Rockets*, Vol. 38, No. 6, 2001, pp. 803–810. doi:10.2514/2.3768

[20] Davidson, J., Lallman, F., McMinn, J. D., Martin, J., Pahle, J., Stephenson, M., Selmon, J., and Bose, D., "Flight Control Laws for NASA's Hyper-X Research Vehicle," AIAA Paper 1999-4124, 1999.

[21] Tournes, C., Landrum, D. B., Shtessel, Y., and Hawk, C. W., "Ramjet-Powered Reusable Launch Vehicle Control by Sliding Modes," *Journal of Guidance, Control, and Dynamics*, Vol. 21, No. 3, 1998, pp. 409–415. doi:10.2514/2.4273

[22] Xu, H., Mirmirani, M., and Ioannou, P., "Adaptive Sliding Mode Control Design for A Hypersonic Flight Vehicle," *Journal of Guidance, Control, and Dynamics*, Vol. 27, No. 5, 2004, pp. 829–838. doi:10.2514/1.12596

[23] Marrison, C., and Stengel, R., "Design of Robust Control Systems for a Hypersonic Aircraft," *Journal of Guidance, Control, and Dynamics*, Vol. 21, No. 1, 1998, pp. 58–63. doi:10.2514/2.4197

[24] Wang, Q., and Stengel, R., "Robust Nonlinear Control of a Hypersonic Aircraft," *Journal of Guidance, Control, and Dynamics*, Vol. 23, No. 4, 2000, pp. 577–585. doi:10.2514/2.4580

[25] Menon, P. K., "Comment on 'Robust Nonlinear Control of a Hypersonic Aircraft'," *Journal of Guidance, Control, and Dynamics*, Vol. 24, No. 1, 2001, p. 143. doi:10.2514/2.4690

[26] Bolender, M. A., and Doman, D. B., "Flight Path Angle Dynamics of Air-Breathing Hypersonic Vehicles," AIAA Paper 2006-6692, 2006.

[27] Parker, J. T., Serrani, A., Yurkovich, S., Bolender, M. A., and Doman, D. B., "Control-oriented Modeling of an Air-Breathing Hypersonic Vehicle," *Journal of Guidance, Control, and Dynamics*, Vol. 30, No. 3, 2007, pp. 856–869. doi:10.2514/1.27830

[28] Fiorentini, L., Serrani, A., Bolender, M., and Doman, D., "Nonlinear Robust/Adaptive Controller Design for an Air-Breathing Hypersonic Vehicle Model," AIAA Paper 2007-6329, 2007.

[29] Fiorentini, L., Serrani, A., Bolender, M. A., and Doman, D. B., "Robust Nonlinear Sequential Loop Closure Control Design for an Air-Breathing Hypersonic Vehicle Model," *Proceedings of the 2008 American Control Conference*, American Automatic Control Council, Dayton, OH, June 2008,pp. 3458–3463.

[30] Williams, T., Bolender, M. A., Doman, D. B., and Morataya, O., "An Aerothermal Flexible Mode Analysis of a Hypersonic Vehicle," AIAA Paper 2006-6647, 2006.

[31] Krstic, M., Kokotovic, P., and Kanellakopoulos, I., *Nonlinear and Adaptive Control Design*, Wiley, New York, NY, 1995, pp. 489–492, 511–514.

[32] Schierman, J.,Ward, D., Hull, J., Gandhi, N., Oppenheimer, M., and Doman, D., "Integrated Adaptive Guidance and Control for Re-Entry Vehicles with Flight-Test Results," *Journal of Guidance, Control, and Dynamics*, Vol. 27, No. 6, 2004, pp. 975–988. doi:10.2514/1.10344

[33] Meirovitch, L., *Analytical Methods in Vibration*, MacMillan, New York, 1967, pp. 135–143, 161–163.

[34] Khalil, H. K., *Nonlinear Systems*, 3rd ed., Prentice–Hall, Upper Saddle River, NJ, 2002, pp. 322–325, 534.

[35] Isidori, A., *Nonlinear Control Systems*, 3rd ed., Springer–Verlag, Berlin, 1995, pp. 219–241, 293–312.